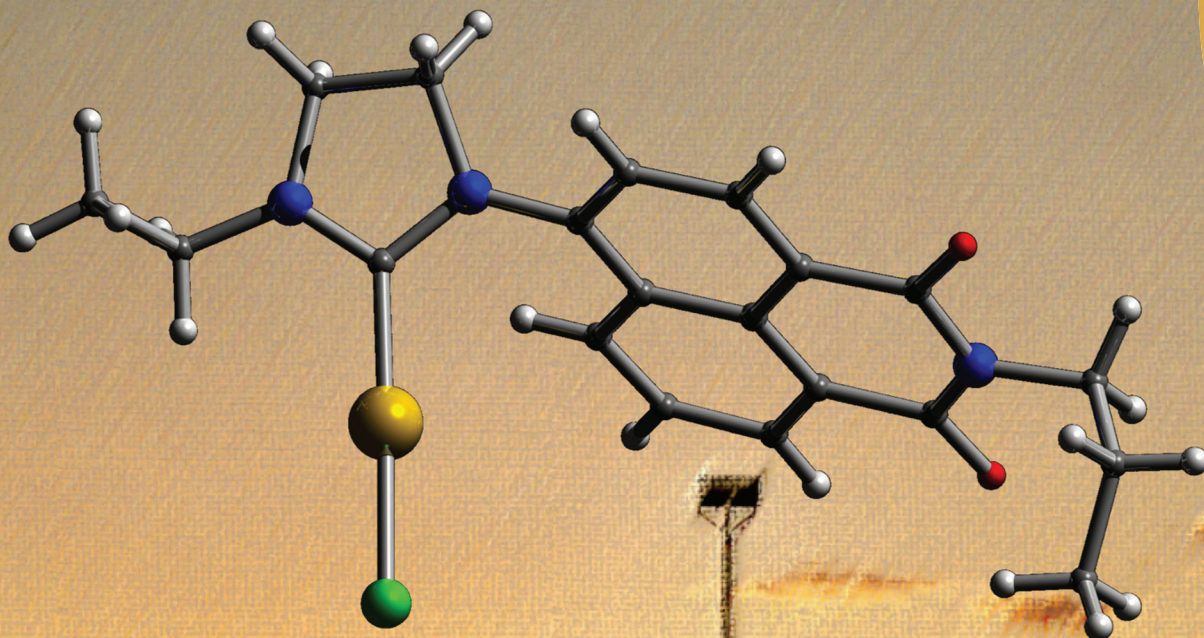


Dalton Transactions

An international journal of inorganic chemistry

rsc.li/dalton



B I O I M A G I N G

ISSN 1477-9226



ROYAL SOCIETY
OF CHEMISTRY

Celebrating
IYPT 2019



PAPER

Simon J. A. Pope *et al.*
Fluorescent functionalised naphthalimides and their
Au(I)–NHC complexes for potential use in cellular
bioimaging



Cite this: *Dalton Trans.*, 2019, **48**, 1599

Fluorescent functionalised naphthalimides and their Au(I)–NHC complexes for potential use in cellular bioimaging†‡

Lara M. Groves,^a Catrin F. Williams,^b Anthony J. Hayes,^c Benjamin D. Ward,^a Marc D. Isaacs,^c Nadine O. Symonds,^a David Lloyd,^c Peter N. Horton,^d Simon J. Coles ^d and Simon J. A. Pope ^{*a}

A series of cationic, dihydroimidazolinium-functionalized 1,8-naphthalimide fluorophores have been isolated as their hexafluorophosphate salts, **[HL]PF₆**. These pro-ligands react with [AuCl(tht)] in the presence of base to form N-heterocyclic carbene (NHC) complexes, **[AuCl(L)]**. Two X-ray structures represent a pro-ligand and complex pairing: the latter reveals the two-coordinate linear geometry of the NHC–Au(I) species, as well as intermolecular interactions supported by both ligand π – π stacking and a weak aurophilic interaction of 3.3205(6) Å. The luminescence properties of the pro-ligands and complexes are dominated by the ICT character of the substituted fluorophore at ca. 500 nm, which is further modulated via functionalization at the 4-position of the naphthalimide. Cytotoxicity assessments were performed for all **[HL]PF₆** and **[AuCl(L)]** species against LOVO, MCF-7, A549 and PC3 cell lines; added lipophilicity seems to correlate with increased cytotoxicity. Confocal fluorescence microscopy was undertaken on a selected **[HL]PF₆** and **[AuCl(L)]** species and showed that the intracellular distribution is dependent upon the specific ligand structure. More detailed co-localisation studies show that selected examples present a predominant lysosomal staining pattern. FLIM studies exemplified the applicability of these probes, and secondly suggest that fluorescence lifetime could be used to provide information on the integrity of the complex and thus liberation of gold in a biological environment.

Received 10th October 2018,
Accepted 21st November 2018

DOI: 10.1039/c8dt04069a

rsc.li/dalton

Introduction

Although the use of gold in medicinal chemistry (known as chrysotherapy)¹ has been recognised for millennia, recent developments have renewed interest in gold's use in metallo-drugs. The variety of Au(I) complexes used in a clinical setting are those incorporating thiolate or phosphine ligands.² The most widely utilised are auranofin, sodium aurothiomalate

and sodium aurothioglucose, all of which have been applied to the treatment of inflammatory autoimmune conditions such as rheumatoid arthritis.³ Auranofin is also under investigation as a treatment to reduce the viral reservoir of HIV that lies latent in the body's T-cells.⁴ The mechanism of biological action of such clinical treatments remains extremely difficult to unravel.⁵ Over the last two decades, there have been several reports suggesting that a variety of Au(I) complexes possess antiproliferative properties *in vitro* against selected human tumour cell lines.⁶

One must consider that the gold agents used clinically are not luminescent compounds and thus other, invasive and analytical techniques are required to understand the intracellular distribution of the gold.⁷ To support such studies, it is helpful therefore if the gold species in question is inherently luminescent, thus enabling non-invasive visualisation of live cells through fluorescence microscopy techniques.⁸

Whilst fluorescence wavelength and Stokes' shift are important parameters for the application of probes to fluorescence microscopy, the use of time-resolved analyses *via* fluorescence lifetime imaging microscopy (FLIM) can provide even more detailed information. This current work describes the synthesis and characterisation of a series of dihydroimidazolinium func-

^aSchool of Chemistry, Main Building, Cardiff University, Cardiff CF10 3AT, UK.
E-mail: popesj@cardiff.ac.uk; Fax: +44 (0)29-20874030; Tel: +44 (0)29-20879316

^bSchool of Engineering, Cardiff University, Cardiff, UK CF24 3AA

^cSchool of Biosciences (and Bio-imaging Research Hub), Sir Martin Evans Building, Cardiff University, Cardiff, UK CF19 3AX

^dUK National Crystallographic Service, Chemistry, Faculty of Natural and Environmental Sciences, University of Southampton, Highfield, Southampton, SO17 1BJ England, UK

†Information on the data underpinning the results presented here, including how to access them, can be found in the Cardiff University data catalogue at <http://doi.org/10.17035/d.2018.0064817469>.

‡Electronic supplementary information (ESI) available: DFT Cartesian coordinates of all calculated structures in a format for convenient visualization; details of all excited states and examples of NMR spectra. CCDC 1831224 and 1831225 for **[HL]PF₆** and **[AuCl(L)]**. For ESI and crystallographic data in CIF or other electronic format see DOI: 10.1039/c8dt04069a



tionalised 1,8-naphthalimide fluorophores which can be deprotonated to act as N-heterocyclic carbene (NHC) donors for coordination to Au(I). These new species are shown to be fluorescent in the visible region and show excellent utility as cell imaging agents including application to FLIM studies of MCF-7 cells. Importantly, the results suggest that fluorescence lifetime is significantly modulated by the presence of the coordinated Au(I), and thus provides further information on the integrity of intracellular metal–ligand complexes.

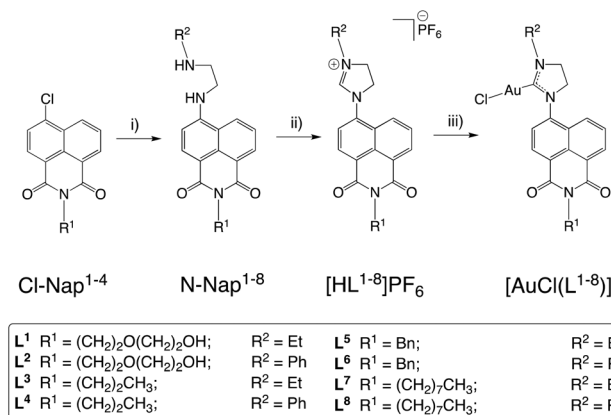
Results and discussion

Synthesis

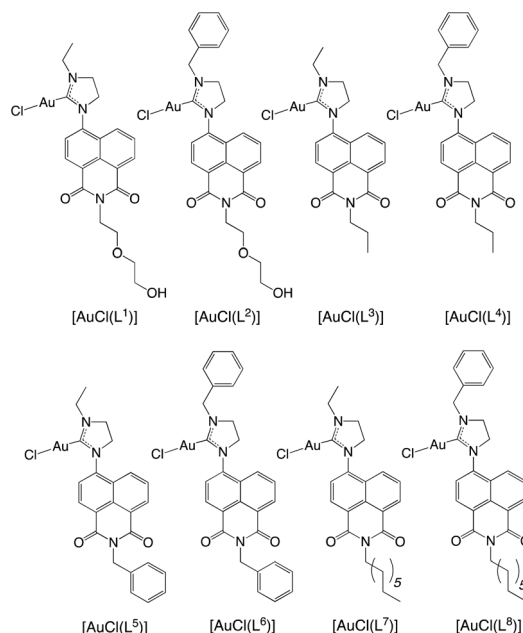
The intermediates **Cl-Nap** and **N-Nap**, pro-ligands **[HL]PF₆** and complexes **[AuCl(L)]** are shown in Scheme 1. The di-substituted dihydroimidazolium pro-ligand salts, **[HL]PF₆**, were synthesized in three steps from commercially available 4-chloro-1,8-naphthalic anhydride. Reaction at the naphthalimide ring of **Cl-Nap** using either *N*-ethylethylenediamine or *N*-phenylethylenediamine (thus $R^2 = \text{Et}$ or Ph) gave the intermediate species, **N-Nap**. Subsequent ring closure of the **N-Nap** species using triethylorthoformate (both as reagent and solvent) in the presence of ammonium hexafluorophosphate yielded the cationic dihydroimidazolium pro-ligands as their hexafluorophosphate salt, **[HL]PF₆**. The corresponding gold(I) complexes, **[AuCl(L)]**, were synthesised from **[AuCl(tht)]** (tht = tetrahydrothiophene) *via* deprotonation of the pro-ligand to yield the NHC Au(I) complex. Despite repeated attempts we were unable to isolate **[AuCl(L⁵)]** in sufficient quantities to allow unequivocal characterisation and further study. The yielded complexes (Scheme 2) are thus based upon an unsymmetrical substitution of a NHC donor at Au(I) that incorporates a conjugated 1,8-naphthalimide fluorophore.

Spectroscopic characterisation of ligands and complexes

¹H NMR spectra for **N-Nap**^{1–8} provided confirmation of substitution at the naphthalimide ring: in most cases, a character-



Scheme 1 Synthetic route: (i) $\text{EtNH}(\text{CH}_2)_2\text{NH}_2$, DMSO, heat; (ii) $\text{CH}(\text{OEt})_3$, NH_4PF_6 , heat; (iii) **[AuCl(tht)]**, KO^tBu , MeOH.



Scheme 2 Structures of the fluorescent Au(I) complexes targeted in this work.

istic *NH* resonance was noted *ca.* 6.0–6.5 ppm, which was assigned to the naphthalimide secondary amine substituent. Upon cyclisation to form the pro-ligands **[HL^{1–8}]PF₆**, the corresponding ¹H NMR spectra showed subtle changes in the chemical shifts of the dihydroimidazolium ethyl backbone; in most cases these were observed as multiplets *ca.* 4.0–4.5 ppm. The *NH* resonance at 6.0–6.5 ppm also disappeared, and a new downfield peak at 9.0–10.0 ppm was assigned to the deshielded H2 position of the imidazolium moiety: both observations were consistent with cyclisation. IR spectra of **[HL^{1–8}]PF₆** showed $\nu(\text{C}=\text{O})$ *ca.* 1650 cm^{-1} and $\nu(\text{PF}_6)$ *ca.* 830 cm^{-1} consistent with the formation of the salts. HRMS were obtained for all intermediates and pro-ligands.

The Au(I) complexes were again characterised by a range of spectroscopic and analytical techniques. ¹H NMR spectra provided clear evidence of coordination to Au(I) through the absence of the downfield H2 imidazolium resonance, and changes in the chemical shifts associated with the ethyl protons in the backbone of the NHC unit. ¹³C{¹H} NMR spectra revealed resonances that correlated with the presence of the different R_1 and R_2 groups. In addition, two unique carbonyl resonances around 162–165 ppm were observed, consistent with the unsymmetrical nature of the 1,8-naphthalimide unit. A downfield signal *ca.* 192–195 ppm (Fig. S1, ESI[†]) was assigned to the Au(I)-coordinated NHC carbon and is comparable with previous studies on Au(I)–NHC complexes which incorporate a saturated NHC backbone.⁹

DFT calculations were employed to further support this ¹³C{¹H} NMR assignment, in which the NMR shielding constants were computed using the gauge including atomic orbital (GIAO) method.¹⁰ Sarotti and Pellegrinet¹¹ have



suggested that a judicious choice of reference compound gives superior chemical shift predictions, and to this end, since the carbene carbon can be considered sp^2 -hybridized, benzene was used as the reference standard and its shielding constants computed at the same level of theory as the carbene complexes. Using these calculations, the δ_C values of the coordinated carbene are predicted to be 192.1 ppm and 192.7 ppm for $[\text{AuCl}(\text{L}^3)]$ and $[\text{AuCl}(\text{L}^4)]$ respectively, both of which compare very favorably to the experimental data thus providing further evidence that the assignments are reliable.

HRMS data were also obtained for the complexes, often correlating with the formation of a cationic complex fragment (through loss of a chloride ligand, or addition of a cation such as Na^+ or NH_4^+). Each spectrum was consistent with retention of the Au-NHC unit. IR spectra confirmed the presence of the ligand, primarily *via* the naphthalimide $\nu(\text{C}=\text{O})$ bands *ca.* 1600–1650 cm^{-1} .

X-ray crystallography

During the synthesis of the ligands and complexes, diffraction quality crystals of $[\text{HL}^3]\text{PF}_6$ and $[\text{AuCl}(\text{L}^3)]$ were isolated. The crystals were obtained by the vapour diffusion of diethyl ether into either a concentrated solution of $[\text{HL}^3]\text{PF}_6$ (acetone) or $[\text{AuCl}(\text{L}^3)]$ (acetonitrile). Data collection parameters are shown in Table S1 (ESI †), together with supporting bond length and bond angle data (Table 1). The resultant structures of $[\text{HL}^3]\text{PF}_6$ and $[\text{AuCl}(\text{L}^3)]$ are shown in Fig. 1 and 2. The structure of the complex (Fig. 1) shows an approximately linear (the C1–Au1–Cl1 angle is $173.76(6)^\circ$) two-coordinate geometry at Au(i). As expected, the C–N bond lengths within the dihydroimidazolium moiety are extended upon coordination to Au(i). The Au–C bond length is $1.984(2)$ Å and thus comparable with structurally related NHC complexes of Au(i).⁹ The structure of $[\text{AuCl}(\text{L})]$ also reveals intermolecular π – π stacking interactions between neighbouring naphthalimide units (Fig. 2). Additional intermolecular interactions are also evident through an Au(i)–Au(i) distance of $3.31459(15)$ Å, which is at the weaker limit of an aurophilic interaction.¹²

Electronic properties and DFT calculations

Solution state UV-vis. absorption and luminescence spectra were obtained for all pro-ligands and complexes (Table 2). The absorption spectra (MeCN) of the pro-ligands were characterised by shorter wavelength peaks (<300 nm) which are assigned to $\pi \rightarrow \pi^*$ transitions associated with the naphthalimide chromophore and phenyl substituents. Between

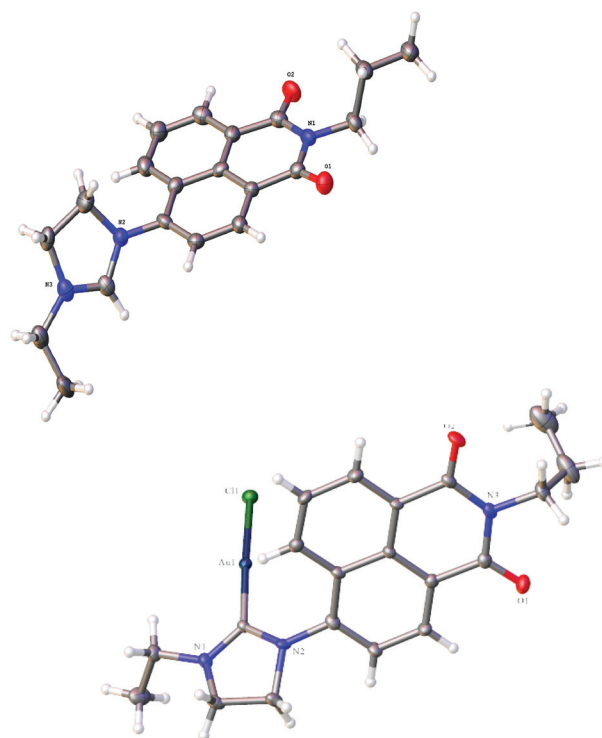


Fig. 1 Crystal structures of $[\text{HL}^3]\text{PF}_6$ (top) and $[\text{AuCl}(\text{L}^3)]$ (bottom). Ellipsoids drawn at 50% probability and counterion omitted for $[\text{HL}^3]\text{PF}_6$.

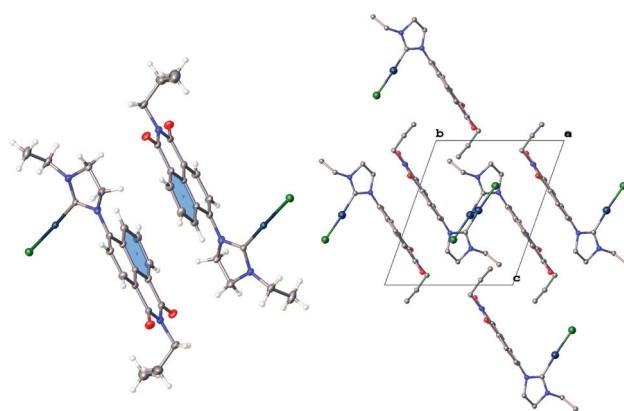


Fig. 2 Representations of the crystal structure of $[\text{AuCl}(\text{L}^3)]$. The π – π packing interactions where the angle between these two planes is 0.00 (19°), the centroid–centroid distance is $3.8001(17)$ Å and the shift distance is $1.644(3)$ Å.

Table 1 Selected bond lengths for $[\text{HL}^3]\text{PF}_6$ and $[\text{AuCl}(\text{L}^3)]$

$[\text{HL}^3]\text{PF}_6$	Bond	$[\text{AuCl}(\text{L}^3)]$	Bond
N(2)–C(16)	1.318(7)	N(1)–C(1)	1.359(2)
N(3)–C(16)	1.299(7)	N(2)–C(1)	1.318(3)
		Au(1)–C(1)	1.984(2)
		Au(1)–Cl(1)	2.2933 (5)
		Au(1)–Au(1')	3.31459 (15)

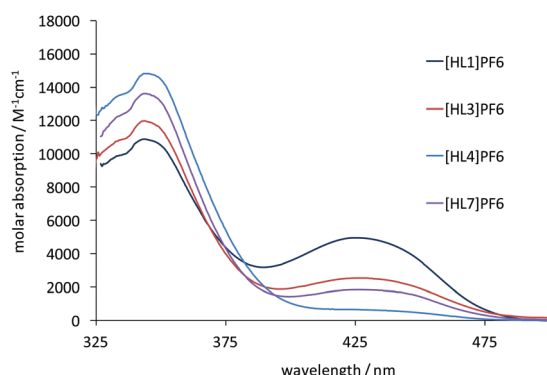
300–450 nm the spectra also revealed weaker features due to different $n \rightarrow \pi^*$ transitions including an intramolecular charge transfer (ICT) localised on the naphthalimide unit. The wavelength of the ICT band was relatively insensitive, firstly, to the nature of the imide (R^1) substituent, and secondly, the R^2 group on the dihydroimidazolium group (Fig. 3). However, the ethyl variants ($[\text{HL}^1]\text{PF}_6$, $[\text{HL}^3]\text{PF}_6$, $[\text{HL}^5]\text{PF}_6$, $[\text{HL}^7]\text{PF}_6$) all showed substantial hyperchromic shifts in the ICT band relative to their phenyl ($[\text{HL}^2]\text{PF}_6$, $[\text{HL}^4]\text{PF}_6$, $[\text{HL}^6]\text{PF}_6$, $[\text{HL}^8]\text{PF}_6$)



Table 2 Absorption and emission data for the proligands and complexes^a

	λ_{abs}^a / nm	λ_{em}^b / nm	τ_{obs}^c / ns	ϕ^d / %
[HL ¹]PF ₆	344, 426	504	7.3	4
[HL ²]PF ₆	342, 429	507	8.7	28
[HL ³]PF ₆	344, 426	502	9.1	4
[HL ⁴]PF ₆	344, 351, 432	503	7.2	4
[HL ⁵]PF ₆	344, 428	502	8.4	31
[HL ⁶]PF ₆	343, 435	504	8.8	17
[HL ⁷]PF ₆	344, 427	501	4.7	5
[HL ⁸]PF ₆	345, 433	503	9.0	12
[AuCl(L ¹)]	344, 351, 436	507	7.8 (45%), <1.0 (55%)	2
[AuCl(L ²)]	349, 433	487	7.2 (78%), 2.8 (22%)	9
[AuCl(L ³)]	345, 351, 439	500	1.1 (76%), <1.0 (24%)	1
[AuCl(L ⁴)]	354, 352	504	6.9 (33%), <1.0 (67%)	1
[AuCl(L ⁶)]	343, 436	503	8.3 (82%), 2.6 (18%)	2
[AuCl(L ⁷)]	345, 351, 439	499	4.3 (9%), 1.0 (91%)	1
[AuCl(L ⁸)]	344, 351, 441	504	<1.0	8

^a Measurements obtained in aerated 10⁻⁵ M acetone solutions. ^b λ_{ex} = 405 nm. ^c λ_{ex} = 372 nm. ^d Using aerated MeCN solution of [Ru(bipy)₃](PF₆)₂ as a reference.

**Fig. 3** A comparison of the UV-vis. absorption spectra for selected pro-ligands (recorded in acetone).

analogues. This may be due to the relative electron donating ability of the R² substituent.

Overall, when compared to other 4-amino-substituted 1,8-naphthalimides,¹³ the absorptivity of the ICT bands in these pro-ligands is relatively diminished and hypsochromically shifted. This is attributed to the cationic nature of the dihydroimidazolium moiety, which may well modulate the overall donor ability of the nitrogen atom at the 4-position of the naphthalimide chromophore. The absorption spectra of the related Au(i) complexes were thus dominated by the ligand-centred transitions. In general, a hypochromic shift of the ICT band relative to the pro-ligand was noted, again probably relating to the net donating ability of the ligated NHC substituent.

DFT calculations

To further probe the electronic properties of the substituted naphthalimide species, the structures of two pro-ligands [HL³]⁺ and [HL⁴]⁺ were calculated using density functional methods, and were subsequently used to probe the underlying

electronic basis for the electronic absorption spectra. The structure of the ethyl congener [HL³]⁺ was compared to that obtained using X-ray data, and was found to provide good agreement between experiment and theory.

Using these optimized structures for TD-DFT calculations gave a particularly noteworthy result: the low energy ICT band, experimentally observed at 425–430 nm, was not obtained in the calculations. We initially rationalized that the band *ca.* 350 nm might correspond to this transition, but with a large computational-experimental discrepancy. TD-DFT often underestimates transitions with a significant CT character,¹⁴ however, this hypothesis would involve an overestimation of the excited state energy, which is apparently contrary to known limitations in this area. Moreover, whilst the phenyl derivative [HL⁴]⁺ contains some CT character (*vide infra*), the ethyl derivative does not. In our earlier work, we have noticed that the accuracy of excited state calculations is only slightly dependent on basis set, but varies considerably with functional. Therefore, the calculations were performed using a number of functionals, namely CAM-B3LYP, B3LYP, PBE0, LC-wPBE, B3PW91, M06, and M06-2X. The lowest energy excited state varied between 291 nm (LC-wPBE) and 353 (B3LYP) for the ethyl derivative [HL³]⁺.

Upon comparison with the experimental spectra, it became apparent that the lowest energy transition corresponded to the experimental band at *ca.* 340–350 nm, and the low-energy band at 425 nm is not replicated in the TD-DFT calculations. One of the significant limitations of DFT calculations can be the lack of counterion or discrete solvent interactions with the substrate; attempts were made to model these, by introducing the anion, and solvent molecules (water and acetone) hydrogen bonding to the appropriate polar groups in the naphthalimide cation, but in every case only a slight (up to 10 nm) variation in the low energy excitation energy was observed.

TD-DFT calculations were performed using the PBE0 hybrid functional, since this allows a closer comparison to related theoretical studies on 1,8-naphthalimides.¹⁵ In this regard, the calculations were in good agreement with the experimental data, since the computed energies were 342 nm ([HL³]⁺) and 348 nm ([HL⁴]⁺) versus 344 nm (for [HL³]PF₆) and 351 nm (for [HL⁴]PF₆). These maxima are in excellent agreement with the experimental data, and moreover the slight red-shift, experimentally observed for [HL⁴]⁺, is replicated (simulated spectra are provided in Fig. 4). The molar absorption coefficients have been estimated from the oscillator strengths using established methods,¹⁶ and their magnitudes agree with the experimentally observed values and are consistent with the expected π - π^* transitions. Experimentally, the phenyl derivative has a higher absorptivity coefficient than the ethyl, which is replicated in the calculations. A further analysis of the excited states indicates that they correspond to π - π^* transitions between the HOMO and LUMO; the HOMO and LUMO of [HL⁴]⁺ are displayed in Fig. 5. The principal difference between the HOMO of [HL³]⁺ and [HL⁴]⁺ is that there is a significant orbital coefficient corresponding to the phenyl group in [HL⁴]⁺; the LUMOs of [HL³]⁺ and [HL⁴]⁺ are essentially identi-



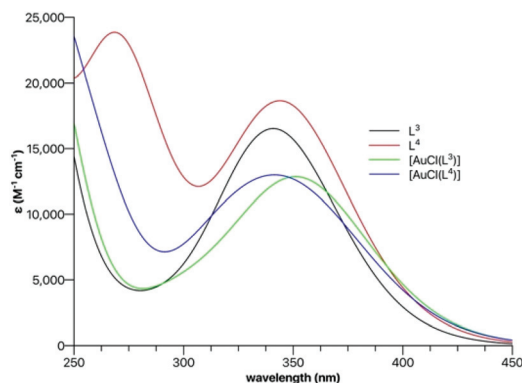


Fig. 4 Simulated UV-vis. absorption spectra of $[\text{HL}^3]^+$ (black), $[\text{HL}^4]^+$ (red), $[\text{AuCl}(\text{L}^3)]$ (green), and $[\text{AuCl}(\text{L}^4)]$ (blue) using TD-DFT data [PBE0: 6-311+G(d,p)/SDD].

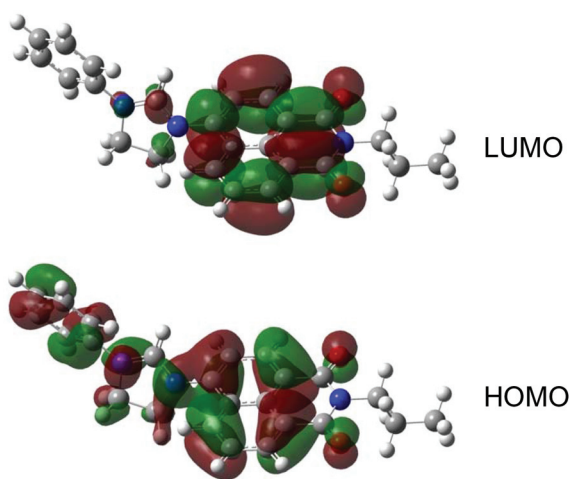


Fig. 5 Calculated HOMO and LUMO of $[\text{HL}^4]^+$ [PBE0/6-311+G(d,p)].

cal, with no significant orbital coefficient over the phenyl ring in $[\text{HL}^4]^+$. This difference in the HOMOs explains the subtle difference in intensity and excitation energy, with the longer excitation wavelength in $[\text{HL}^4]^+$ corresponding to the greater HOMO delocalization in $[\text{HL}^4]^+$, compared to $[\text{HL}^3]^+$.

The nature of the low energy bands do not change significantly upon coordination of the pro-ligands to Au(I), in that they are still dominated by HOMO–LUMO π – π^* transitions. However, the maxima are predicted to undergo a small red-shift, which replicates the experimentally observed spectra. A comparison of the HOMO and LUMO orbital energies in the pro-ligands and complexes reveals that both HOMO and LUMO increase in energy as a result of coordination to the Au centre, but that the increase in the HOMO energies is marginally more than that found for the LUMO; for example in $[\text{HL}^3]^+$ the HOMO and LUMO lie at -7.32 eV and -3.06 eV respectively, and at -6.91 eV and -2.73 eV in $[\text{AuCl}(\text{L}^3)]$. This has the effect of reducing the HOMO–LUMO difference in the complex to 4.18 eV from 4.26 eV in the imidazolium precursor. A similar observation is found for $[\text{HL}^4]^+$, for which the HOMO–

LUMO energy difference decreases from 4.22 eV to 4.13 eV in $[\text{AuCl}(\text{L}^4)]$.

Fluorescence properties

The fluorescence properties of the ligands and complexes were assessed at room temperature in aerated acetone solution (Table 1). Irradiation with 405 nm (corresponding to the excitation line for confocal fluorescence microscopy) relates to excitation of the ICT absorption band. For the pro-ligands this yielded a broad structureless emission peak (Fig. 6) at around 490 – 510 nm with a corresponding lifetimes in the range 4 – 10 ns, consistent with previous reports on amino-functionalized 1,8-naphthalimides of this type.¹³ The variation in imide substituent had minimal influence upon emission wavelength (Fig. 6). Quantum yields were 4 – 31% implying some relatively bright fluorophores within the series. It was also noted that these species showed excitation wavelength dependent emission wavelengths: excitation at 345 nm, which corresponds to one of the π – π^* absorptions gave a higher energy emission at *ca.* 440 nm, which is assumed to correlate with emission from a π – π^* excited state.

For the complexes, irradiation at 405 nm again generally revealed a ligand-based ICT peak *ca.* 500 nm, but in some cases an additional peak or shoulder at higher energies (440 – 450 nm) was also noted (Fig. 7). Again, this shorter wavelength peak was enhanced by using excitation at 345 nm. Comparison of the fluorescent lifetimes and quantum yield values for the complexes with the corresponding free ligands generally indicated a partial quenching of the ICT emission in the presence of a coordinated, heavy atom. For example, in the case of $[\text{AuCl}(\text{L}^3)]$ the fluorescence lifetime was dominated by a very short lifetime component *ca.* 1 ns, contrasting with, and differentiated from, the value obtained for $[\text{HL}^3]\text{PF}_6$ (Fig. 7).

Cytotoxicity and bioimaging studies

Au(I) NHC complexes have been the focus of several studies examining biological applications, including mitochondria-targeted, anti-tumour,¹⁷ and antimicrobial¹⁸ examples. Fine-tuning of the ligand architecture has allowed the development

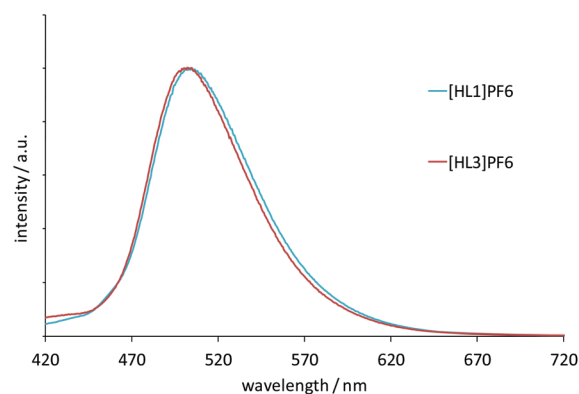


Fig. 6 Normalised steady state emission spectra of selected ligands excited at 405 nm (recorded in aerated acetone).



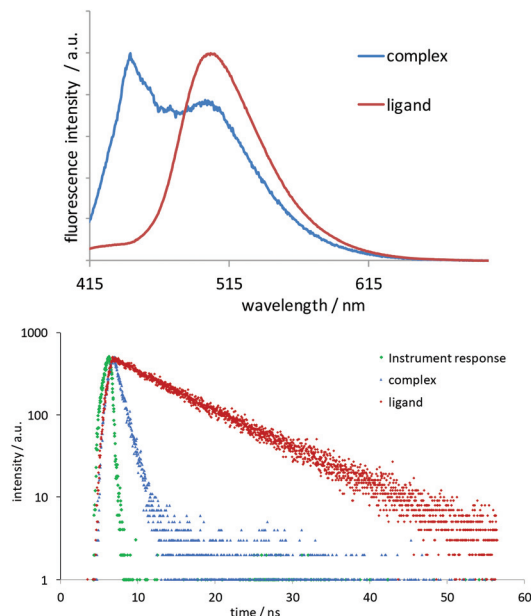


Fig. 7 Top: Normalised emission spectra of selected complexes excited at 405 nm (recorded in aerated acetone). Bottom: Time-resolved measurements showing the comparative decay profiles for ligand $[\text{HL}^3]\text{PF}_6$ (red) and complex $[\text{AuCl}(\text{L}^3)]$ (blue) against the instrument response (green).

of lipophilic, cationic Au(I)–NHC complexes that selectively induce apoptosis in cancer cells and show selective targeting of mitochondrial selenoproteins, such as TrxR.¹⁹ Fluorophore-tethered Au(I)–NHC compounds have demonstrated apoptosis in cancer cells,²⁰ as well as DNA binding capability.²¹ Au(I) NHC frameworks provide an excellent basis for the development of anticancer agents.²²

Prior to any imaging work, cytotoxicity assessments were obtained for complexes and pro-ligands using the MTT assay (Table 3). Data were recorded for four cancer cell lines: LOVO, A549, PC3 and MCF-7, the latter for correlation with the imaging studies. The data clearly revealed that the uncharged

complexes were less toxic to LOVO, A549 and PC3 cells than the corresponding cationic pro-ligands. This is in contrast to our previous findings which have shown that gold complexes of the type $[\text{Au}(\text{PPh}_3)(\text{L})]$ can often have enhanced cytotoxicity *versus* the free ligand, attributed to the presence of lipophilicity enhancing co-ligands (e.g. PPh_3) at Au(I).²³ The importance of charge has also been noted in cytotoxic iridium(III) complexes, with cationic species proving more toxic to cell lines²⁴ and Gram positive bacteria²⁵ than neutral analogues. For the pro-ligands, $[\text{HL}^6]\text{PF}_6$ was the least toxic with IC_{50} values $>100 \mu\text{M}$ for each cell type. In contrast, closely related $[\text{HL}^5]\text{PF}_6$ was the most toxic, with strong activity against LOVO, PC3 and MCF-7s. Highly lipophilic $[\text{HL}^7]\text{PF}_6$ also showed strong activity against LOVO and MCF-7. Overall the results showed that relatively minor changes in the molecular structures had a profound influence upon the cytotoxicity.

A limited number of Au(I) complexes incorporating fluorescent ligands have been reported²⁶ for cellular imaging, although the fluorescent properties of such species are not always optimal for microscopy. Therefore, cellular microscopy studies including FLIM were undertaken with one of the pro-ligand/complex pairings, $[\text{HL}^3]\text{PF}_6$ and $[\text{AuCl}(\text{L}^3)]$, using MCF-7 cells. Fluorophore concentrations of $100 \mu\text{g ml}^{-1}$ (i.e. comparable to the IC_{50} values) and more dilute 10 ng ml^{-1} (well below the obtained IC_{50} values) in DMSO were used for $[\text{HL}^3]\text{PF}_6$ and $[\text{AuCl}(\text{L}^3)]$. In all cases the cells were irradiated with 405 nm excitation which matches well with the ICT absorption band of these naphthalimide-based fluorophores; detection wavelengths were 500–550 nm.

Firstly, $[\text{HL}^3]\text{PF}_6$ demonstrated rapid uptake ($<30 \text{ min}$) and internalisation by the MCF-7 cells (Fig. 8). Cytoplasmic fluorescence was concentrated in well-defined spheroidal volumes consistent with organelle localisation. There was no evidence of nuclear sequestration. The corresponding complex $[\text{AuCl}(\text{L}^3)]$ also showed reasonable uptake internalisation with bright foci of fluorescence observable within the cytoplasm, but not the nucleus (Fig. S2, ESI†).

More distinct localisation was observed for both $[\text{HL}^3]\text{PF}_6$ and $[\text{AuCl}(\text{L}^3)]$ at a diluted probe concentration of 10 ng ml^{-1}

Table 3 IC_{50} (μM) values (standard deviation in parentheses) for the pro-ligands and complexes against four cancer cell lines

Compound	LOVO	A549	PC3	MCF-7
$[\text{HL}^1]\text{PF}_6$	30.07(3.19)	33.62(5.09)	56.40(3.08)	68.35(3.95)
$[\text{HL}^2]\text{PF}_6$	73.36(2.36)	>100	98.1(3.91)	66.83(2.85)
$[\text{HL}^3]\text{PF}_6$	42.75(8.66)	56.83(4.06)	71.27(2.89)	61.21(3.02)
$[\text{HL}^4]\text{PF}_6$	51.81(5.34)	75.68(1.10)	72.82(3.03)	56.38(2.84)
$[\text{HL}^5]\text{PF}_6$	7.27(1.19)	47.10(0.55)	8.58(0.03)	7.12(0.36)
$[\text{HL}^6]\text{PF}_6$	>100	>100	>100	>100
$[\text{HL}^7]\text{PF}_6$	5.22(2.49)	53.95(1.41)	42.00(5.69)	9.98(4.77)
$[\text{HL}^8]\text{PF}_6$	>100	>100	>100	33.23(5.84)
$[\text{AuCl}(\text{L}^1)]$	68.94(2.29)	>100	>100	84.21(11.38)
$[\text{AuCl}(\text{L}^2)]$	91.64(3.20)	>100	>100	62.88(5.58)
$[\text{AuCl}(\text{L}^3)]$	>100	>100	>100	48.58(10.58)
$[\text{AuCl}(\text{L}^4)]$	41.54(2.88)	>100	>100	27.79(11.89)
$[\text{AuCl}(\text{L}^6)]$	49.10(7.97)	>100	>100	46.21(13.01)
$[\text{AuCl}(\text{L}^7)]$	50.92(6.20)	>100	46.63(0.71)	41.75(9.34)
$[\text{AuCl}(\text{L}^8)]$	40.99(11.08)	>100	>100	4.82(0.77)

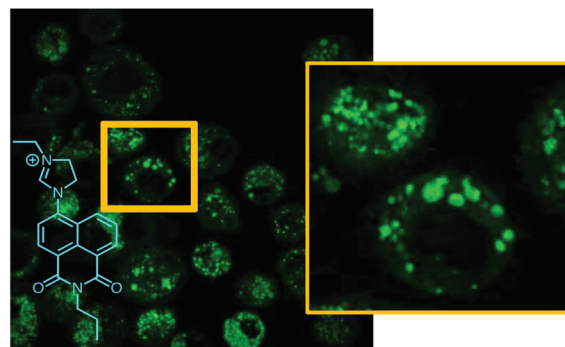


Fig. 8 Confocal fluorescence microscopy images of MCF-7 cells incubated with $[\text{HL}^3]\text{PF}_6$ showing localized signals ($\lambda_{\text{ex}} = 405 \text{ nm}$ and $\lambda_{\text{em}} = 525 \text{ nm}$). Cells incubated with $100 \mu\text{g ml}^{-1}$ of the fluorophore.



(1:10 000 dilution when compared to the preliminary microscopy studies). Under these conditions, co-localisation studies were investigated using commercial fluorophores for staining of mitochondrial, endoplasmic reticulum (ER), Golgi and lysosomal compartments (Fig. 9 and Fig. S3 and S4, ESI†). Fig. 9 shows the obtained superimposed images with $[\text{HL}^3]\text{PF}_6$ and $[\text{AuCl}(\text{L}^3)]$ respectively, and colocalisation is clearly evident (as indicated by the yellow-orange colouration) only with the lysosomal stain, LysoTracker Deep Red. A recently reported acridine-functionalized Au(I) compound has also shown lysosomal localisation.²⁰

Having fully elucidated the intracellular localisation of both probes, FLIM analyses was applied to MCF-7 cells which had been incubated with $[\text{HL}^3]\text{PF}_6$ and $[\text{AuCl}(\text{L}^3)]$. For FLIM, the cells were imaged *via* a pulsed 440 nm diode laser excitation source, which is again well matched to the ICT absorption band of the naphthalimide fluorophores, and data collection was facilitated through time correlated single photon counting. Decay curves were fitted using an *n*-exponential tail fit, while applying an estimated instrument response function. In all cases the lowest χ^2 square value was obtained by modelling three components to the exponential decay.

For $[\text{HL}^3]\text{PF}_6$, the FLIM images (Fig. 10) show the localised hot spots of fluorescence which were earlier attributed to lysosomal localisation. From the data analyses of the image, the dominant lifetime component was obtained as 9.2 ns. This value compares favourably (*cf.* 9.1 ns) with the solution state spectroscopic measurements (Table 1), validating the data fitting protocol. This value also implies that the fluorescence labelling of the lysosomal compartments of the cell can be clearly attributed to $[\text{HL}^3]\text{PF}_6$ and that the intrinsic structure of the fluorophore is intact following incubation with the cells.

In the case of MCF-7 cells incubated with $[\text{AuCl}(\text{L}^3)]$, good quality FLIM images were again obtained. In this case, the fitted parameters suggest a dominant lifetime of *ca.* 11 ns

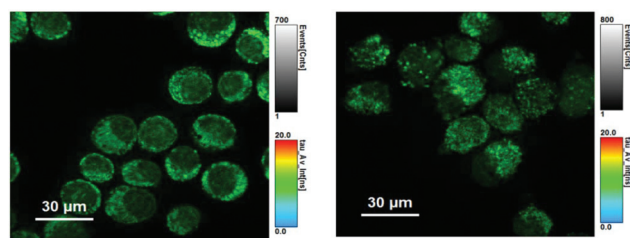


Fig. 10 FLIM images of MCF-7 cells incubated with $[\text{HL}^3]\text{PF}_6$ (left) and $[\text{AuCl}(\text{L}^3)]$ (right) using pulsed excitation at 440 nm. Fitted parameters for left image: $\tau_1 = 9.2$ ns (77%), $\tau_2 = 3.4$ ns (20%), $\tau_3 = 0.4$ ns (3%); for right image, $\tau_1 = 11.0$ ns (68%), $\tau_2 = 3.9$ ns (25%), $\tau_3 = 0.5$ ns (7%).

(Fig. 10). This value is significantly longer than that spectroscopically obtained (1.1 ns), but more comparable with the fluorescence lifetime for $[\text{HL}^3]\text{PF}_6$. Therefore, the FLIM data suggests that the gold complex may dissociate under biological conditions to regenerate the dihydroimidazolium-like fluorophore. In these cases, the fluorescence lifetime obtained from FLIM might be indicative of such an intracellular process.

The data from these microscopy measurements suggests that further work is required to understand the speciation of these Au(I) carbene complexes within a biological environment. In particular, it is important to consider the acidic nature of lysosomal compartments and the effect that this may have on such complexes. Since the solubility of $[\text{AuCl}(\text{L}^3)]$ is limited to organic solvents it has not been possible to elucidate the pH dependent stability of this species, but previous studies have noted how the gold–carbene bond can tolerate acidic conditions at elevated temperatures.²⁷ Further, our studies have shown that such complexes are stable >6 h in DMSO (incubated at 37 °C) solutions in the absence of light, as indicated by ¹³C NMR data (retention of coordinated carbene). However, it is well known that Au(I) carbene complexes can display photoinduced decomposition.²⁸ Therefore one must exercise caution when seeking to correlate cytotoxicity data with confocal fluorescence microscopy imaging. Further work is required to unravel the influence that light irradiation may have upon the speciation and toxicity of gold(I) complexes within a cell.

Conclusions

The stepwise synthesis of a range of 4-substituted 1,8-naphthalimide derivatives that incorporate a dihydroimidazolium cationic unit give fluorescent species with emission dominated by an ICT emission band around 500 nm. Once deprotonated, these dihydroimidazolium salts can be utilised as NHC ligands for Au(I) to form complexes. In all cases, the fluorescence of these complexes is again dominated by the ligand, but often partially quenched by the presence of Au(I) leading to the possibility of discriminating ligand/complex pairings on the basis of fluorescence lifetime. The varying functionality of the ligands led to different cytotoxicity profiles across cancer

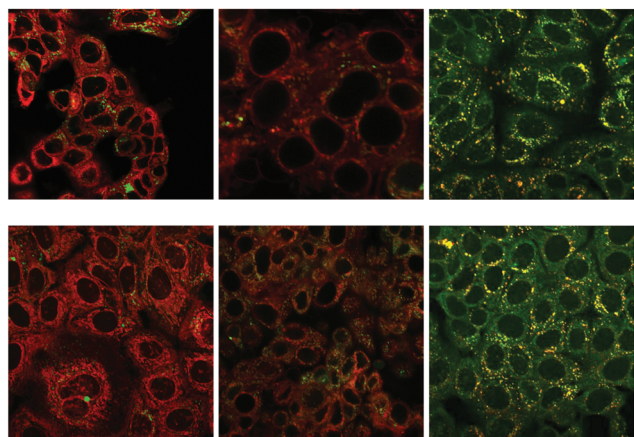


Fig. 9 Confocal fluorescence microscopy images of MCF-7 cells incubated with $[\text{HL}^3]\text{PF}_6$ (top) and $[\text{AuCl}(\text{L}^3)]$ (bottom). Representative superimposed images where yellow-orange signifies co-localisation (from left to right) with an ER stain, Golgi stain and lysosomal stain. Note strong lysosomal fluorescence co-localisation.



cell lines, with the cationic pro-ligands proving generally more toxic than the corresponding complexes. Selected ligands and complexes were incubated with MCF-7 cells and fluorescence microscopy was undertaken, showing that these fluorophores are biocompatible. More detailed colocalisation studies were conducted on a ligand/complex pairing and identified that the species show definitive localisation in lysosomes. Finally, we have shown that the ICT fluorescence lifetime of these species can be utilised in FLIM. Lifetime imaging studies on $[\text{AuCl}(\text{L}^3)]$ indicate that this species probably dissociates from gold within the cell. Further studies are now required to fully elucidate the possible mechanism for this process, but FLIM appears to be a potential imaging tool for supporting such investigations.

Experimental

General considerations

All reagents and solvents were commercially available and were used without further purification if not stated otherwise. For the measurement of ^1H , ^{31}P , and ^{13}C NMR spectra a Bruker Fourier³⁰⁰ (300 MHz), Bruker AVANCE HD III equipped with a BFFO SmartProbeTM (400 MHz) or Bruker AVANCE III HD with BBO Prodigy CryoProbe (500 MHz) was used. The obtained chemical shifts δ are reported in ppm and are referenced to the residual solvent signal. Spin-spin coupling constants J are given in Hz.

Low-resolution mass spectra were obtained by the staff at Cardiff University. High-resolution mass spectra were carried out at the EPSRC National Mass Spectrometry Facility at Swansea University. High resolution mass spectral (HRMS) data were obtained on a Waters MALDI-TOF mx at Cardiff University or on a Thermo Scientific LTQ Orbitrap XL by the EPSRC UK National Mass Spectrometry Facility at Swansea University. IR spectra were obtained from a Shimadzu IR-Affinity-1S FTIR. Reference to spectroscopic data are given for known compounds. UV-Vis studies were performed on a Shimadzu UV-1800 spectrophotometer as MeCN solutions (2.5 or 5×10^{-5} M). Photophysical data were obtained on a JobinYvon-Horiba Fluorolog spectrometer fitted with a JY TBX picosecond photodetection module as MeCN solutions. Quantum yield measurements were obtained on aerated MeCN solutions of the complexes using $[\text{Ru}(\text{bpy})_3](\text{PF}_6)_2$ in aerated MeCN as a standard ($\Phi = 0.016$).²⁹ Emission spectra were uncorrected and excitation spectra were instrument corrected. The pulsed source was a Nano-LED configured for 295 nm or 372 nm output operating at 1 MHz. Luminescence lifetime profiles were obtained using the JobinYvon-Horiba FluoroHub single photon counting module and the data fits yielded the lifetime values using the provided DAS6 deconvolution software.

X-ray diffraction

For both samples, a suitable crystal³⁰ was selected and mounted on a MITIGEN holder in oil on a Rigaku FRE+ (45.0

kV, 55.0 mA) equipped with HF Varimax confocal mirrors (70 μm focus) and an AFC12 goniometer and HG Saturn 724+ detector ($[\text{HL}^3]\text{PF}_6$) or a HyPix 6000 detector ($[\text{AuCl}(\text{L}^3)]$). The crystals were kept at $T = 100(2)$ K during data collection. Data were measured using profile data from ω -scans using MoK α radiation. Cell determination and data collection were carried out using CrystalClear³¹ ($[\text{HL}^3]\text{PF}_6$) or CrystalisPro³² ($[\text{AuCl}(\text{L}^3)]$). With the data reduction, cell refinement and absorption correction using CrystalisPro. Using Olex2,³³ the structures were solved with the ShelXT³⁴ structure solution program and the models were refined with version 2014/7 of ShelXL³⁵ using Least Squares minimisation. All non-hydrogen atoms were refined anisotropically. Hydrogen atom positions were calculated geometrically and refined using the riding model. For sample $[\text{HL}^3]\text{PF}_6$, the PF_6 anion was disordered over two positions and for $[\text{AuCl}(\text{L}^3)]$ the propyl chain was disordered over two positions. As such various geometrical (SADI) and displacement (SIMU, RIGU) restraints were applied to the disordered atoms. **Diffraction:** Rigaku AFC12 goniometer equipped with an enhanced sensitivity (HG) Saturn724+ detector mounted at the window of an FR-E+ SuperBright molybdenum rotating anode generator with VHF Varimax optics (70 μm focus). **Cell determination and data collection:** CrystalClear-SM Expert 3.1 b27 (Rigaku, 2013). **Data reduction, cell refinement and absorption correction:** CrystalisPro. **Structure solution:** SUPERFLIP.³⁶ For sample L^3 , the PF_6 anion was disordered over two positions. As such various geometrical (SAME) and displacement (SIMU) restraints were applied.

Cytotoxicity assessment via MTT assay

The cytotoxicity of the complexes was assessed using the colourimetric and quantitative MTT [3-(4,5-dimethylthiazol-2-yl)-2,5-diphenyltetrazolium bromide] assay, first reported by Mosmann.³⁷ Quantification was achieved using a multi-well scanning spectrophotometer and reported as an IC_{50} value.

Method for cytotoxicity analysis

Anti-tumor evaluation in MCF7, LOVO, A549 and PC3 cell lines was performed by MTT assay. Compounds were prepared as 0.1–100 mM stock solutions dissolved in DMSO and stored at -20°C . Cells were seeded into 96-well microtitre plates at a density of 5×10^3 cells per well and allowed 24 h to adhere. Decimal compound dilutions were prepared in medium immediately prior to each assay (final concentration 0.1–100 μM). Experimental medium was DMEM +10% FCS (PC3 and Lovo) or RPMI +10% heat inactivated FCS (A549 and MCF7). Following 96 h compound exposure at 37°C , 5% CO_2 , MTT reagent (Sigma Aldrich) was added to each well (final concentration 0.5 mg ml^{-1}). Incubation at 37°C for 4 h allowed reduction of MTT by viable cells to an insoluble formazan product. MTT was removed and formazan solubilized by addition of 10% Triton X-100 in PBS. Absorbance was read on a Tecan Sunrise spectrophotometer at 540 nm as a measure of cell viability; thus inhibition relative to control was determined (IC_{50}) from four independent sets of data and the standard deviations calculated from these data sets.



Confocal imaging of MCF-7 cells

Cell culture. All cell culture reagents were purchased through Sigma Aldrich. MCF-7 cells were grown on circular glass coverslips for 5–7 days in RPMI-1640 medium, supplemented with heat inactivated 5% foetal bovine serum and 100 U ml⁻¹ penicillin/streptomycin solution, until around 70–90% confluent. For experiments, culture medium was replaced with 1 ml fresh RPMI-1640 and the cells then incubated with either 100 µg ml⁻¹ or 10 ng ml⁻¹ of probe in DMSO. A range of commercially available organelle probes (ThermoFisher) were used for co-localisation studies with the above compounds in live cells: mitochondria were labelled with TMRE (tetramethylrhodamine ethyl ester) 200 nM; $\lambda_{\text{ex}} = 549$ nm; $\lambda_{\text{em}} = 575$ nm; cell membranes and lipid droplets with HCS LipidTOX Red Neutral Lipid Stain (1 : 1000 dilution from the commercial kit; $\lambda_{\text{ex}} = 577$ nm; $\lambda_{\text{em}} = 609$ nm); the endoplasmic reticulum with ER Tracker red (1 µM; $\lambda_{\text{ex}} = 587$ nm; $\lambda_{\text{em}} = 615$ nm); the Golgi apparatus with BODIPY TR ceramide (5 µM; $\lambda_{\text{ex}} = 590$ nm; $\lambda_{\text{em}} = 620$ nm) and lysosomes with LysoTracker Red (1 µM; $\lambda_{\text{ex}} = 577$ nm; $\lambda_{\text{em}} = 590$ nm). All fluorescent compounds were incubated for 30 minutes at 37 °C then washed in warmed PBS before imaging.

Confocal microscopy. MCF-7 cells were imaged using an LSM880 Airyscan confocal microscope system (Zeiss, Germany) equipped with time correlated single photon counting (TCSPC) for fluorescence lifetime imaging (FLIM; PicoQuant GmbH, Germany). For fluorescence localisation studies, cells were imaged using appropriate excitation and emission settings for detection of either the naphthalimide-based probes alone, or either probe together with a commercial co-localisation agent (see above) using Zen software (Zeiss, Germany). Differential interference contrast (DIC) optics were used to simultaneously record cell morphology alongside the fluorescence signal. For co-localisation studies, sequential fluorescence image acquisition was used to avoid spectral crosstalk between the dyes. For FLIM, the probes were imaged *via* a pulsed 440 nm diode laser using SymphoTime software (PicoQuant GmbH, Germany) for TCSPC. Decay curves were fitted using an *n*-exponential tail fit, applying an estimated instrument response function (IRF). A decent fit was accepted provided the fitted curve overlaid well with the decay curve; the χ^2 square value was ~ 1 and the residual values spread randomly around 0; selecting the least number of model parameters (*n*) in each case. Fluorescence lifetime measurements of the probes were displayed as fitted lifetime image maps.

Density functional calculations

Calculations were performed using the Gaussian 09 program.³⁸ Calculated structures were optimized without symmetry constraints and the nature of the stationary point verified using a frequency calculation; in all cases no imaginary frequencies were observed. The PBE0³⁹ functional was used along with the 6-311+G(d,p) triple- ζ basis set⁴⁰ on all centres except for Au, for which the Stuttgart-Dresden basis set was used with a relativistic effective core potential.⁴¹ Solvent was

included in all calculations as the polarized continuum model, with the molecular cavity defined by a united atom model that incorporates hydrogen into the parent heavy atom.⁴² TD-DFT calculations were carried out with at the same level of theory as the geometry optimizations; the first 24 excited states were calculated. NMR shielding constants were computed using the gauge including atomic orbital method incorporated into Gaussian 09;¹⁰ ¹³C chemical shifts were computed relative to benzene ($\delta_{\text{C}} = 129.2$ ppm).

Reagents and precursors

Cl-Nap derivatives⁴³ and [AuCl(tht)]⁴⁴ were prepared according to the literature. All other reagents were used as received and general and standard precautions were taken during their handling and manipulation.

Ligands and precursors

Synthesis of N-Nap¹. Cl-Nap¹ (502 mg, 1.6 mmol) and *N*-ethylethylenediamine (0.64 ml, 6.3 mmol) were heated for 48 hours at 100 °C in DMSO under a nitrogen atmosphere. The solution was cooled and water (15 ml) added. The solution was neutralised using 1 M HCl and then extracted into DCM. The organic phase was washed with water, dried over MgSO₄, and the solvent removed to yield the product as an orange solid (yield: 125 mg, 22%). ¹H NMR (400 MHz, CDCl₃): δ_{H} 8.51 (d, 1H, ³*J*_{HH} = 7.2 Hz), 8.30 (d, 1H, ³*J*_{HH} = 8.4 Hz), 8.09 (d, 1H, ³*J*_{HH} = 8.5 Hz), 7.48 (app. t, 1H, ³*J*_{HH} = 7.7 Hz), 6.51 (d, 1H, ³*J*_{HH} = 8.4 Hz), 6.35 (br. t, 1H), 4.36 (t, 2H, ³*J*_{HH} = 5.2 Hz), 3.81 (t, 2H, ³*J*_{HH} = 8.1 Hz), 3.70–3.60 (m, 4H), 3.35 (t, 2H, ³*J*_{HH} = 5.8 Hz), 3.02 (t, 2H, ³*J*_{HH} = 5.8 Hz), 2.69 (q, 2H, ³*J*_{HH} = 7.1 Hz), 1.13 (t, 3H, ³*J*_{HH} = 7.1 Hz) ppm. HRMS found *m/z* 372.1919, calcd *m/z* 372.1918 for [C₂₀H₂₆N₃O₄]⁺.

Synthesis of [HL¹]PF₆. N-Nap¹ (100 mg, 0.27 mmol) and NH₄PF₆ (49 mg, 0.3 mmol) were heated at 100 °C in HC(OEt)₃ for 3 h under a nitrogen atmosphere. The solution was cooled and the solvent decanted to leave an orange colored oil. Et₂O (2 × 10 ml) was then added and slowly decanted and the remaining oil dried *in vacuo* to yield [HL¹]PF₆ as an orange oil (77 mg, 54%). ¹H NMR (300 MHz, (CD₃)₂CO): δ_{H} 8.97 (s, 1H), 8.59 (dd, 1H, *J*_{HH} = 8.5, 3.4 Hz), 8.55–8.46 (m, 2H), 8.00 (dd, 1H, *J*_{HH} = 7.5, 2.3 Hz), 7.95–7.86 (m, 1H), 4.80 (t, 2H, ³*J*_{HH} = 9.9 Hz), 4.50 (t, 2H, ³*J*_{HH} = 10.5 Hz), 4.24 (t, 2H, ³*J*_{HH} = 6.2 Hz), 3.90 (q, 2H, ³*J*_{HH} = 7.3 Hz), 3.73–3.66 (m, 2H), 3.58–3.52 (m, 2H), 2.03–1.99 (m, 2H), 1.47 (t, 3H, ³*J*_{HH} = 7.3 Hz) ppm. ¹³C{¹H} NMR (101 MHz, (CD₃)₂CO): δ_{C} 158.2, 138.6, 131.7, 130.8, 128.7, 128.4, 127.1, 124.1, 123.4, 72.4, 70.2, 69.6, 67.3, 61.1, 53.0, 49.3, 44.1, 39.2, 39.1, 14.6, 12.0 ppm. UV/Vis ((CH₃)₂CO): λ_{max} /nm (ϵ /M⁻¹ cm⁻¹) = 426 (4960), 344 (10 920). HRMS found *m/z* 382.1752, calcd *m/z* 382.1761 for [C₂₁H₂₄N₃O₄]⁺. IR (solid) ν /cm⁻¹: 2978, 2947, 2875, 1697, 1651, 1581, 1503, 1462, 1450, 1346, 1157, 1123, 1090, 1057, 825, 783, 754, 739, 556, 422, 405, 392.

Synthesis of N-Nap². As for N-Nap¹, but using Cl-Nap¹ (502 mg, 1.6 mmol) and *N*-phenylethylenediamine (0.82 ml, 6.2 mmol). The product was isolated as a yellow solid (yield: 260 mg, 66%). ¹H NMR (400 MHz, CDCl₃): δ_{H} 8.37 (d, 1H,



$^3J_{\text{HH}} = 7.3$ Hz), 8.28 (d, 1H, $^3J_{\text{HH}} = 8.7$ Hz), 8.09 (d, 1H, $^3J_{\text{HH}} = 8.3$ Hz), 7.44 (app. t, 1H, $^3J_{\text{HH}} = 7.4$ Hz), 7.30 (m, 2H), 7.01–6.93 (m, 2H), 6.54 (d, 1H, $^3J_{\text{HH}} = 8.3$ Hz), 6.11 (s, 1H), 4.38 (t, 2H, $^3J_{\text{HH}} = 4.9$ Hz), 3.87 (t, 2H, $^3J_{\text{HH}} = 4.7$ Hz), 3.77–3.62 (overlapping m, 8H) ppm.

Synthesis of [HL²]PF₆. As for [HL¹]PF₆, but using **N-Nap²** (198 mg, 0.47 mmol) and NH₄PF₆ (82 mg, 0.52 mmol). The product was precipitated from CHCl₃ and Et₂O giving a yellow powder (yield: 129 mg, 64%). ¹H NMR (400 MHz, (CD₃)₂CO): δ_{H} 9.85 (s, 1H), 8.85 (d, 1H, $^3J_{\text{HH}} = 8.5$ Hz), 8.77–8.62 (m, 2H), 8.30 (d, 1H, $^3J_{\text{HH}} = 7.8$ Hz), 8.06 (dd, 1H, $J_{\text{HH}} = 15.5, 7.9$ Hz), 7.72 (d, 2H, $^3J_{\text{HH}} = 7.7$ Hz), 7.63 (d, 2H, $^3J_{\text{HH}} = 7.5$ Hz), 7.56–7.43 (m, 1H), 5.23–4.98 (m, 4H), 4.37 (t, 2H, $^3J_{\text{HH}} = 6.2$ Hz), 3.89–3.71 (overlapping m, 8H) ppm. ¹³C{¹H} NMR (101 MHz, (CD₃)₂CO): δ_{C} 164.2, 163.7, 157.2, 138.8, 137.0, 132.7, 131.6, 130.9, 130.5, 129.9, 129.7, 129.6, 128.9, 128.0, 125.9, 124.9, 124.3, 119.8, 73.3, 71.0, 68.20, 61.9, 54.6, 50.8, 40.2 ppm. UV/Vis ((CH₃)₂CO): λ_{max} /nm ($\epsilon/\text{M}^{-1} \text{cm}^{-1}$) 429 (1000), 342 (9700). HRMS ES[−] found m/z 430.1756, calcd m/z 430.1761 for [C₂₅H₂₄N₃O₄]⁺. IR (solid) ν/cm^{-1} : 3010, 2932, 2810, 1699, 1654, 1626, 1581, 1492, 1379, 1348, 1269, 1234, 1142, 1128, 1097, 1057, 829, 785, 754, 736, 689, 556, 410.

Synthesis of Cl-Nap². 4-Chloro-1,8-naphthalic anhydride (3 g, 12.9 mmol) and propylamine (1.9 ml, 25.8 mmol) were heated at reflux in EtOH for 24 hours under a nitrogen atmosphere. The solution was cooled to room temperature and stored at −20 °C for 24 hours. The resulting precipitate was filtered to yield **Cl-Nap²** as a bright yellow solid (yield: 2.74 g, 78%). ¹H NMR (400 MHz, CDCl₃): δ_{H} 8.59 (d, 1H, $^3J_{\text{HH}} = 7.3$ Hz), 8.53 (d, 1H, $^3J_{\text{HH}} = 8.5$ Hz), 8.42 (d, 1H, $^3J_{\text{HH}} = 7.9$ Hz), 7.82–7.73 (m, 2H), 4.08 (t, 2H, $^3J_{\text{HH}} = 7.6$ Hz), 1.70 (app. sext., 2H, $^3J_{\text{HH}} = 7.5$ Hz), 0.95 (t, 3H, $^3J_{\text{HH}} = 7.4$ Hz) ppm.

Synthesis of N-Nap³. As for **N-Nap¹**, but using **Cl-Nap²** (491 mg, 1.8 mmol) and *N*-ethylethylenediamine (0.76 ml, 7.2 mmol). The product was obtained as an orange solid (yield: 0.573 g, 98%). ¹H NMR (500 MHz, CDCl₃): δ_{H} 8.51 (d, 1H, $^3J_{\text{HH}} = 8.2$ Hz), 8.38 (d, 1H, $^3J_{\text{HH}} = 8.4$ Hz), 8.14 (d, 1H, $^3J_{\text{HH}} = 8.4$ Hz), 7.55 (app. t, 1H, $^3J_{\text{HH}} = 8.2$ Hz), 6.61 (d, 1H, $^3J_{\text{HH}} = 8.4$ Hz), 6.29 (br. t, 1H), 4.08–4.03 (m, 2H), 3.41–3.36 (m, 2H), 3.06–3.01 (m, 2H), 2.69 (q, 2H, $^3J_{\text{HH}} = 7.1$ Hz), 1.69 (q, 2H, $^3J_{\text{HH}} = 7.5$ Hz), 1.12 (t, 3H, $^3J_{\text{HH}} = 5.1$ Hz), 0.94 (t, 3H, $^3J_{\text{HH}} = 7.4$ Hz) ppm. HRMS found m/z 326.1866, calcd m/z 326.1863 for [C₂₉H₂₄N₃O₂]⁺.

Synthesis of [HL³]PF₆. As for [HL¹]PF₆, but using **N-Nap³** (346 mg, 1.1 mmol) and NH₄PF₆ (190 mg, 1.2 mmol). The product was obtained as an orange coloured oil (yield: 0.254 g, 50%). ¹H NMR (400 MHz, (CD₃)₂CO): δ_{H} 8.94 (s, 1H), 8.58–8.47 (m, 3H), 7.97 (d, 1H, $^3J_{\text{HH}} = 7.8$ Hz), 7.88 (app. t, 1H, $^3J_{\text{HH}} = 7.9$ Hz), 4.65 (t, 2H, $^3J_{\text{HH}} = 10.0$ Hz), 4.45 (t, 2H, $^3J_{\text{HH}} = 11.1$ Hz), 3.82 (q, 2H, $^3J_{\text{HH}} = 7.3$ Hz), 1.66–1.52 (m, 2H), 1.07–0.96 (m, 3H), 0.85 (t, 3H, $^3J_{\text{HH}} = 7.5$ Hz) ppm. ¹³C{¹H} NMR (101 MHz, (CD₃)₂CO): δ_{C} 164.0, 163.5, 156.0, 139.3, 132.4, 131.5, 129.8, 129.6, 129.3, 127.9, 125.0, 124.2, 124.2, 53.9, 50.1, 45.0, 42.4, 21.9, 12.9, 11.7 ppm. UV/Vis ((CH₃)₂CO): λ_{max} /nm ($\epsilon/\text{M}^{-1} \text{cm}^{-1}$) = 426 (2520), 344 (11 980). HRMS found m/z 336.1709, calcd m/z 336.1707 for [C₂₀H₂₂N₃O₂]⁺. IR (solid) ν/cm^{-1} : 3381, 3089,

2968, 1697, 1651, 1591, 1514, 1443, 1429, 1408, 1389, 1350, 1269, 1234, 1201, 1155, 1086, 1069, 962, 891, 876, 825, 789, 760, 738, 556, 463, 434, 409.

Synthesis of N-Nap⁴. As for **N-Nap¹**, but using **Cl-Nap²** (767 mg, 2.8 mmol) and *N*-phenylethylenediamine (1.5 ml, 11.2 mmol). The product was yielded as an orange solid (yield: 1.00 g, 97%). ¹H NMR (400 MHz, (CD₃)₂CO): δ_{H} 8.42 (d, 1H, $^3J_{\text{HH}} = 8.5$ Hz), 8.35 (d, 1H, $^3J_{\text{HH}} = 7.2$ Hz), 8.21 (d, 1H, $^3J_{\text{HH}} = 8.5$ Hz), 7.52 (app. t, 1H, $^3J_{\text{HH}} = 8.2$ Hz), 6.98 (app. t, 2H, $^3J_{\text{HH}} = 8.2$ Hz), 6.76 (d, 1H, $^3J_{\text{HH}} = 8.5$ Hz), 6.58 (d, 2H, $^3J_{\text{HH}} = 8.0$ Hz), 6.48 (br. t, 1H), 5.15 (br. t, 1H, NH), 3.93 (t, 2H, $^3J_{\text{HH}} = 7.5$ Hz), 3.62 (t, 2H, $^3J_{\text{HH}} = 5.8$ Hz), 3.47 (t, 2H, $^3J_{\text{HH}} = 6.0$ Hz), 1.58 (q, 2H, $^3J_{\text{HH}} = 7.5$ Hz), 0.81 (t, 3H, $^3J_{\text{HH}} = 7.5$ Hz) ppm.

Synthesis of [HL⁴]PF₆. As for [HL¹]PF₆, but using **N-Nap⁴** (750 mg, 2.0 mmol) and NH₄PF₆ (360 mg, 2.2 mmol). Product was obtained as a yellow solid (yield: 860 mg, 81%). ¹H NMR (400 MHz, (CD₃)₂CO): δ_{H} 9.87 (s, 1H), 8.86 (d, 1H, $^3J_{\text{HH}} = 8.5$ Hz), 8.71 (overlapping d, 2H), 8.31 (d, 1H, $^3J_{\text{HH}} = 7.8$ Hz), 8.06 (app. t, 1H, $^3J_{\text{HH}} = 7.9$ Hz), 7.73 (d, 2H, $^3J_{\text{HH}} = 7.6$ Hz), 7.62 (app. t, 2H, $^3J_{\text{HH}} = 7.5$ Hz), 7.50 (app. t, 1H, $^3J_{\text{HH}} = 7.4$ Hz), 5.17–5.08 (m, 4H), 4.12 (t, 2H, $^3J_{\text{HH}} = 7.5$ Hz), 1.78 (q, 2H, $^3J_{\text{HH}} = 7.5$ Hz), 1.00 (t, 3H, $^3J_{\text{HH}} = 7.4$ Hz) ppm. ¹³C{¹H} NMR (101 MHz, (CD₃)₂CO): δ_{C} 164.1, 163.6, 157.2, 138.7, 137.0, 132.6, 131.5, 130.9, 130.8, 129.9, 129.6, 128.9, 128.0, 125.9, 125.1, 124.4, 119.8, 119.6, 119.3, 54.6, 50.9, 42.5, 22.0, 11.7 ppm. UV/Vis ((CH₃)₂CO): λ_{max} /nm ($\epsilon/\text{M}^{-1} \text{cm}^{-1}$) = 351 (14 320), 344 (0.599). HRMS found m/z 384.1700, calcd m/z 384.1707 for [C₂₄H₂₂N₃O₂]⁺. IR (solid) ν/cm^{-1} : 2974, 1699, 1651, 1626, 1585, 1494, 1391, 1364, 1350, 1271, 1236, 1072, 8423, 829, 787, 758, 689, 557, 469, 434.

Synthesis of Cl-Nap³. 4-Chloro-1,8-naphthalic anhydride (1.00 g, 4.3 mmol) and benzylamine (1 ml, 9.2 mmol) were heated in ethanol (70 ml) at reflux under nitrogen for 12 hours. The solution was cooled to room temperature forming a yellow precipitate immediately on freezing. This was filtered and washed with Et₂O (10 ml) to give **Cl-Nap³** as a yellow solid (yield: 1.2 g, 88%). ¹H NMR (500 MHz, CDCl₃): δ_{H} 8.61 (d, 1H, $^3J_{\text{HH}} = 7.3$ Hz), 8.53 (d, 1H, $^3J_{\text{HH}} = 8.5$ Hz), 8.45 (d, 1H, $^3J_{\text{HH}} = 7.8$ Hz), 7.77 (dd, 2H, $J_{\text{HH}} = 17.4, 8.2$ Hz), 7.49 (d, 2H, $^3J_{\text{HH}} = 7.6$ Hz), 7.26 (app. t, 1H, $^3J_{\text{HH}} = 7.4$ Hz), 7.23–7.16 (m, 2H), 5.32 (s, 2H) ppm.

Synthesis of N-Nap⁵. As for **N-Nap¹**, but using **Cl-Nap³** (500 mg, 1.6 mmol) and *N*-ethylethylenediamine (0.65 ml, 6.2 mmol). **N-Nap⁵** was obtained as an orange solid (574 mg, 94%). ¹H NMR (300 MHz, CDCl₃): δ_{H} 8.41 (d, 1H, $J = 7.3$ Hz), 8.29 (d, 1H, $J = 8.4$ Hz), 7.97 (d, 1H, $J = 8.3$ Hz), 7.52–7.37 (m, 3H), 7.25–7.10 (m, 3H), 6.48 (d, 1H, $J = 8.4$ Hz), 6.25 (br. t, 1H), 5.28 (s, 2H), 3.27 (dd, 2H, $J = 10.3, 5.0$ Hz), 2.97 (t, 2H, $J = 5.7$ Hz), 2.65 (q, 2H, $J = 7.1$ Hz), 1.09 (t, 3H, $J = 7.1$ Hz) ppm.

Synthesis of [HL⁵]PF₆. As for [HL¹]PF₆, but using **N-Nap⁵** (389 mg, 1.0 mmol) and ammonium hexafluorophosphate (187 mg, 1.15 mmol). The product [HL⁵]PF₆ was obtained as an orange oil (371 mg, 67%). ¹H NMR (300 MHz, (CD₃)₂CO): δ_{H} 9.00 (s, 1H), 8.63 (d, 1H, $J = 8.5$ Hz), 8.54 (overlapping d, 2H), 8.01 (d, 1H, $J = 7.8$ Hz), 7.94 (app. t, 1H, $J = 7.9$ Hz), 7.44 (d, 2H, $J = 7.3$ Hz), 7.33–7.20 (m, 3H), 5.25 (s, 2H), 4.82 (t, 2H,



$J = 10.4$ Hz), 4.53 (t, 2H, $J = 10.5$ Hz), 3.94 (q, 2H, $J = 7.2$ Hz), 1.52 (t, 3H, $J = 7.4$ Hz) ppm. $^{13}\text{C}\{^1\text{H}\}$ NMR (126 MHz, $(\text{CD}_3)_2\text{CO}$): δ_{C} 163.3, 162.8, 158.0, 138.7, 137.5, 131.8, 131.0, 129.0, 128.5, 128.3, 128.2, 127.2, 127.0, 124.1, 123.1, 123.1, 53.0, 49.3, 44.1, 43.2, 35.2, 23.6, 20.6, 12.0 ppm. UV/Vis $((\text{CH}_3)_2\text{CO})$: $\lambda_{\text{max}}/\text{nm}$ ($\epsilon/\text{M}^{-1}\text{cm}^{-1}$): 428 (3700), 344 (14 560). HRMS found m/z 384.1718, calcd m/z 384.1712 for $[\text{C}_{24}\text{H}_{22}\text{N}_3\text{O}_2]^+$. IR (solid) ν/cm^{-1} : 2372, 2341, 1699, 1651, 1582, 1549, 1497, 1454, 1423, 1381, 1346, 1290, 1234, 1182, 1155, 1072, 1028, 970, 876, 827, 783, 754, 734, 702, 665, 613, 583, 556, 469, 407.

Synthesis of N-Nap⁶. Cl-Nap³ (513 mg, 1.65 mmol) and *N*-phenylethylenediamine (0.83 ml, 6.34 mmol) were heated in DMSO (6 ml) at reflux under nitrogen for 48 hours. The product was cooled and water (6 ml) was added to form yellow precipitate. The reaction solution was neutralised with hydrochloric acid (3 ml, 0.1 M) and filtered. Product was re-precipitated using dichloromethane and Et₂O and then filtered to give a yellow solid (yield: 551 mg, 87%). ^1H NMR (400 MHz, CDCl_3): δ_{H} 8.51 (d, 1H, $^3J_{\text{HH}} = 6.6$ Hz), 8.41 (d, 1H, $^3J_{\text{HH}} = 8.3$ Hz), 7.88 (d, 1H, $^3J_{\text{HH}} = 8.3$ Hz), 7.56 (d, 2H, $^3J_{\text{HH}} = 7.1$ Hz), 7.54–7.48 (m, 1H), 7.30 (app. t, 2H, $^3J_{\text{HH}} = 7.3$ Hz), 7.23 (d, 3H, $^3J_{\text{HH}} = 7.4$ Hz), 6.81 (app. t, 1H, $^3J_{\text{HH}} = 7.4$ Hz), 6.76 (d, 2H, $^3J_{\text{HH}} = 7.6$ Hz), 6.66 (d, 1H, $^3J_{\text{HH}} = 8.4$ Hz), 5.57 (br. t, 1H), 5.35 (s, 2H), 3.61 (overlapping, 4H) ppm.

Synthesis of [HL⁶]PF₆. As for [HL¹]PF₆, but using N-Nap⁶ (346 mg, 0.87 mmol) and NH₄PF₆ (156 mg, 0.97 mmol). The product was obtained as a yellow powder (yield: 322 mg, 85%). ^1H NMR (400 MHz, $(\text{CD}_3)_2\text{CO}$): δ_{H} 9.87 (s, 1H), 8.86 (d, 1H, $^3J_{\text{HH}} = 8.5$ Hz), 8.74–8.68 (m, 2H), 8.30 (d, 1H, $^3J_{\text{HH}} = 7.6$ Hz), 8.06 (app. t, 1H, $^3J_{\text{HH}} = 7.7$ Hz), 7.72 (d, 2H, $^3J_{\text{HH}} = 8.4$ Hz), 7.62 (app. t, 2H, $^3J_{\text{HH}} = 8.2$ Hz), 7.48 (d, 3H, $^3J_{\text{HH}} = 6.7$ Hz), 7.36–7.24 (m, 3H), 5.35 (s, 2H), 5.15–3.90 (m, 6H) ppm. $^{13}\text{C}\{^1\text{H}\}$ NMR (101 MHz, $(\text{CD}_3)_2\text{CO}$): δ_{C} 164.2, 163.7, 157.2, 138.9, 138.4, 137.0, 132.9, 131.8, 130.9, 130.2, 130.0, 129.8, 129.6, 129.2, 129.1, 128.9, 128.2, 128.1, 125.9, 125.2, 125.0, 124.3, 119.8, 54.6, 50.9, 44.2 ppm. UV/Vis $((\text{CH}_3)_2\text{CO})$: $\lambda_{\text{max}}/\text{nm}$ ($\epsilon/\text{M}^{-1}\text{cm}^{-1}$) 435 (400), 343 (5700). HRMS ES[−] found m/z 432.1701, calcd m/z 432.1707 for $[\text{C}_{28}\text{H}_{22}\text{N}_3\text{O}_2]^+$. IR (solid) ν/cm^{-1} : 1699, 1655, 1637, 1589, 1495, 1452, 1387, 1350, 1337, 1290, 1277, 1232, 1182, 959, 881, 839, 825, 791, 756, 748, 700, 689, 557, 472.

Synthesis of Cl-Nap⁴. 4-Chloro-1,8-naphthalic anhydride (3 g, 12.9 mmol) and octylamine (4.26 ml, 25.8 mmol) were heated at reflux in EtOH for 24 hours under a nitrogen atmosphere. The solution was cooled to room temperature and stored at -20 °C for 24 hours and the resulting precipitate filtered. The crude product was dissolved in dichloromethane (30 ml) and washed with 0.1 M HCl (30 ml), followed by H₂O (30 ml) and brine (30 ml). The collected organic phase was dried over MgSO₄, and the solvent removed to yield a yellow solid (yield: 3.78 g, 85%). ^1H NMR (400 MHz, CDCl_3): δ_{H} 8.60 (d, 1H, $^3J_{\text{HH}} = 7.3$ Hz), 8.53 (d, 1H, $^3J_{\text{HH}} = 8.5$ Hz), 8.45 (d, 1H, $^3J_{\text{HH}} = 7.9$ Hz), 7.82–7.75 (m, 2H), 4.11–4.05 (m, 2H), 1.69–1.50 (m, 2H), 1.47–1.12 (overlapping m, 10H), 0.80 (t, 3H, $^3J_{\text{HH}} = 6.7$ Hz) ppm.

Synthesis of N-Nap⁷. As for N-Nap¹, but using Cl-Nap⁴ (600 mg, 1.7 mmol) and *N*-ethylethylenediamine (0.71 ml, 7.0 mmol). The product was obtained as an orange solid (yield: 582 mg, 84%). ^1H NMR (400 MHz, CDCl_3): δ_{H} 8.60 (d, 1H, $^3J_{\text{HH}} = 6.5$ Hz), 8.37 (d, 1H, $^3J_{\text{HH}} = 8.4$ Hz), 8.15 (d, 1H, $^3J_{\text{HH}} = 8.2$ Hz), 7.55 (app. t, 1H, $^3J_{\text{HH}} = 7.6$ Hz), 6.59 (d, 1H, $^3J_{\text{HH}} = 8.4$ Hz), 6.32 (br. t, 1H), 4.07 (t, 2H, $^3J_{\text{HH}} = 7.6$ Hz), 3.40 (q, 2H, $^3J_{\text{HH}} = 4.9$ Hz), 3.05 (t, 2H, $^3J_{\text{HH}} = 5.4$ Hz), 2.71 (q, 2H, $^3J_{\text{HH}} = 7.1$ Hz), 1.66 (m, 2H), 1.40–1.11 (overlapping m, 13H), 0.78 (t, 3H, $^3J_{\text{HH}} = 7.0$ Hz) ppm. HRMS found m/z 396.2644, calcd m/z 396.2646 for $[\text{C}_{24}\text{H}_{34}\text{N}_3\text{O}_2]^+$.

Synthesis of [HL⁷]PF₆. As for [HL¹]PF₆, but using Pro⁷ (476 mg, 1.2 mmol) and NH₄PF₆ (217 mg, 1.3 mmol). The product was obtained as a yellow colored powder (496 mg, 74%). ^1H NMR (500 MHz, $(\text{CD}_3)_2\text{CO}$): δ_{H} 9.06 (s, 1H), 8.69–8.58 (m, 3H), 8.08 (d, 1H, $^3J_{\text{HH}} = 7.8$ Hz), 7.99 (dd, 1H, $J_{\text{HH}} = 8.5, 7.3$ Hz), 4.86 (t, 2H, $^3J_{\text{HH}} = 10$ Hz), 4.57 (t, 2H, $^3J_{\text{HH}} = 10$ Hz), 4.13–4.09 (m, 2H), 3.95 (q, 2H, $^3J_{\text{HH}} = 7.2$ Hz), 2.87 (d, 3H, $^3J_{\text{HH}} = 15.7$ Hz), 1.70 (dt, 2H, $^3J_{\text{HH}} = 15.0, 7.5$ Hz), 1.51 (t, 2H, $^3J_{\text{HH}} = 7.3$ Hz), 1.33–1.24 (m, 6H), 0.87 (t, 3H, $^3J_{\text{HH}} = 6.9$ Hz) ppm. $^{13}\text{C}\{^1\text{H}\}$ NMR (101 MHz, $(\text{CD}_3)_2\text{CO}$): δ_{C} 164.0, 163.5, 158.9, 139.3, 132.4, 131.5, 129.7 (two overlapping environments), 129.5, 129.3, 127.9, 125.0, 124.1, 53.9, 50.1, 45.0, 40.9, 32.5, 30.0, 29.9, 28.6, 27.8, 23.3, 14.3, 12.8 ppm. UV/Vis $((\text{CH}_3)_2\text{CO})$: $\lambda_{\text{max}}/\text{nm}$ ($\epsilon/\text{M}^{-1}\text{cm}^{-1}$) = 427 (1820), 344 (13 620). HRMS found m/z 406.2482, calcd m/z 406.2489 for $[\text{C}_{25}\text{H}_{32}\text{N}_3\text{O}_2]^+$. IR (solid) ν/cm^{-1} : 2959, 2924, 2855, 1703, 1651, 1589, 1508, 1391, 1354, 1254, 1232, 1155, 1093, 827, 785, 754, 555, 416.

Synthesis of N-Nap⁸. As for N-Nap¹, but using Cl-Nap⁴ (503 mg, 1.4 mmol) and *N*-phenylethylenediamine (0.76 ml, 5.8 mmol). The product was isolated as a yellow coloured solid (yield: 601 mg, 65%). ^1H NMR (400 MHz, CDCl_3): δ_{H} 8.55 (d, 1H, $^3J_{\text{HH}} = 6.6$ Hz), 8.43 (d, 1H, $^3J_{\text{HH}} = 8.4$ Hz), 8.03 (d, 1H, $^3J_{\text{HH}} = 8.5$ Hz), 7.61–7.55 (m, 1H), 7.25–7.19 (m, 2H), 6.83 (app. t, 1H, $^3J_{\text{HH}} = 7.4$ Hz), 6.78 (d, 2H, $^3J_{\text{HH}} = 8.5$ Hz), 6.72 (d, 1H, $^3J_{\text{HH}} = 8.4$ Hz), 5.70 (br. s, 1H), 4.17–4.09 (m, 2H), 3.65 (t, 4H, $^3J_{\text{HH}} = 4.3$ Hz), 1.72 (dd, 2H, $J_{\text{HH}} = 15.2, 7.3$ Hz), 1.46–1.20 (m, 10H), 0.86 (t, 3H, $^3J_{\text{HH}} = 6.8$ Hz) ppm.

Synthesis of [HL⁸]PF₆. As for [HL¹]PF₆, but using N-Nap⁸ (497 mg, 1.1 mmol) and NH₄PF₆ (200 mg, 1.2 mmol). The product was obtained as a yellow coloured solid (yield: 274 mg, 54%). ^1H NMR (400 MHz, $(\text{CD}_3)_2\text{CO}$): δ_{H} 9.85 (s, 1H), 8.84 (d, 1H, $^3J_{\text{HH}} = 8.6$ Hz), 8.70 (dd, 2H, $^3J_{\text{HH}} = 7.6, 2.6$ Hz), 8.29 (d, 1H, $^3J_{\text{HH}} = 7.8$ Hz), 8.08–8.03 (m, 1H), 7.72 (d, 2H, $^3J_{\text{HH}} = 7.7$ Hz), 7.62 (app. t, 2H, $^3J_{\text{HH}} = 8.0$ Hz), 7.49 (app. t, 1H, $^3J_{\text{HH}} = 7.4$ Hz), 5.18–4.70 (m, 6H), 4.14 (t, 2H, $^3J_{\text{HH}} = 7.2$ Hz), 1.77–1.66 (m, 2H), 1.45–1.24 (m, 10H), 0.87 (t, 3H, $^3J_{\text{HH}} = 6.9$ Hz) ppm. $^{13}\text{C}\{^1\text{H}\}$ NMR (101 MHz, $(\text{CD}_3)_2\text{CO}$): δ_{C} 164.0, 163.5, 157.1, 138.7, 137.0, 132.6, 131.5, 130.9, 129.8, 129.6, 128.9, 128.0, 125.9, 125.0, 124.4, 119.8, 54.6, 50.8, 41.0, 32.5, 30.5, 30.3, 30.1, 29.9, 28.7, 27.8, 23.3, 14.3 ppm. UV/Vis $((\text{CH}_3)_2\text{CO})$: $\lambda_{\text{max}}/\text{nm}$ ($\epsilon/\text{M}^{-1}\text{cm}^{-1}$) 433 (200), 345 (7200). HRMS found m/z 454.2478, calcd m/z 454.2489 for $[\text{C}_{29}\text{H}_{32}\text{N}_3\text{O}_2]^+$. IR (solid) ν/cm^{-1} : 2922, 2850, 1708, 1697, 1653, 1536, 1589, 1492, 1390, 1352, 1267, 1232, 1095, 831, 785, 754, 734, 686, 557, 464, 405.



Synthesis of [AuCl(L¹)]. [HL¹]PF₆ (81 mg, 0.15 mmol), KO^tBu (17 mg, 0.15 mmol) and [AuCl(tht)] (49 mg, 0.15 mmol) were dissolved in CH₃OH and then heated to reflux, under nitrogen, overnight in the absence of light. The solution was cooled, and then concentrated *in vacuo*, and then Et₂O added dropwise to induce precipitation. [AuCl(L¹)] was yielded as a grey colored solid (yield: 76 mg, 81%). ¹H NMR (400 MHz, CDCl₃): δ_H 8.68–8.59 (m, 2H), 8.25 (d, 1H, ³J_{HH} = 8.7 Hz), 7.83 (app. d, 2H, ³J_{HH} = 7.8 Hz), 4.46 (t, 2H, ³J_{HH} = 4.6 Hz), 4.04–3.81 (m, 6H), 3.73–3.63 (m, 2H), 3.56 (br s, 2H), 3.47 (q, 2H, ³J_{HH} = 6.8 Hz), 1.42 (t, 3H, ³J_{HH} = 7.3 Hz), 1.25 (br s, 1H) ppm. ¹³C{¹H} NMR (126 MHz, CDCl₃): δ_C 193.9, 163.9, 163.7, 132.3, 131.6, 129.1, 128.5, 128.0, 126.2, 123.0, 72.4, 70.4, 70.0, 68.5, 66.8, 62.0, 53.7, 48.7, 46.3, 39.9, 39.4, 15.3, 13.8 ppm. UV/Vis ((CH₃)₂CO): λ_{max}/nm (ε/M^{−1} cm^{−1}) 436 (1420), 351 (4620), 344 (4660). HRMS found *m/z* 636.0918, calcd *m/z* 636.0935 for [C₂₁H₂₃AuClN₃O₄ + Na]⁺. IR (solid) ν/cm^{−1}: 2899, 2666, 2360, 1695, 1653, 1582, 1537, 1510, 1477, 1427, 1379, 1348, 1341, 1265, 1230, 1105, 1043, 835, 785, 737, 669, 600, 581, 556, 455, 444, 436, 428, 420, 409.

Synthesis of [AuCl(L²)]. As for [AuCl(L¹)], but using [HL²]PF₆ (68 mg, 0.16 mmol), [AuCl(tht)] (51 mg, 0.16 mmol) and KO^tBu (18 mg, 0.16 mmol). The product was obtained as a grey-yellow solid (yield: 88 mg, 84%). ¹H NMR (500 MHz, CD₃CN): δ_H 8.66–8.59 (m, 2H), 8.01 (d, 1H, ³J_{HH} = 7.9 Hz), 7.94 (app. t, 1H, ³J_{HH} = 7.9 Hz), 7.82 (d, 2H, ³J_{HH} = 7.9 Hz), 7.53 (d, 2H, ³J_{HH} = 7.8 Hz), 7.43 (d, 2H, ³J_{HH} = 7.6 Hz), 4.39–4.21 (m, 4H), 3.81–3.19 (overlapping m, 10H) ppm. ¹³C{¹H} NMR (126 MHz, CDCl₃): δ_C 192.7, 163.8, 163.6, 132.2, 131.5, 131.4, 129.7, 129.0, 128.2, 128.1, 126.5, 123.4, 123.3, 116.5, 113.9, 72.4, 70.4, 70.0, 68.5, 66.8, 66.0, 62.0, 53.7, 52.3, 52.2, 39.9, 15.4, 15.3 ppm. UV/Vis ((CH₃)₂CO): λ_{max}/nm (ε/M^{−1} cm^{−1}) 433 (900), 349 (8700). HRMS found *m/z* 643.1608, calcd *m/z* 643.1614 for [C₂₅H₂₃AuN₃O₄ + NH₃]⁺. IR (solid) ν/cm^{−1}: 2990, 2880, 1705, 1659, 1593, 1487, 1437, 1408, 1381, 1346, 1337, 1321, 1288, 1234, 1188, 1121, 1049, 887, 843, 789, 756, 692, 559, 482, 451, 438, 426, 419, 405.

Synthesis of [AuCl(L³)]. As for [AuCl(L¹)], but using [HL³]PF₆ (80 mg, 0.17 mmol), KO^tBu (19 mg, 0.17 mmol) and [AuCl(tht)] (53 mg, 0.17 mmol). The reaction mixture was heated overnight at reflux under a nitrogen atmosphere. The product was obtained as an off-white solid (yield: 40 mg, 45%). ¹H NMR (500 MHz, CDCl₃): δ_H 8.55 (dd, 1H, ³J_{HH} = 7.3, 1.0 Hz), 8.52 (d, 1H, ³J_{HH} = 7.7 Hz), 8.21 (d, 1H, ³J_{HH} = 8.4 Hz), 7.76 (d, 1H, ³J_{HH} = 7.7 Hz), 7.73–7.68 (m, 1H), 4.20–4.05 (m, 4H), 3.93 (t, 2H, ³J_{HH} = 9.3 Hz), 3.83 (br s, 2H), 1.76–1.76 (m, 2H), 1.29 (t, 3H, ³J_{HH} = 7.2 Hz), 0.96 (t, 3H, ³J_{HH} = 7.4 Hz) ppm. ¹³C{¹H} NMR (126 MHz, CDCl₃): δ_C 193.5, 163.9, 163.4, 142.9, 131.9, 131.3, 129.4, 129.0, 128.4, 127.9, 126.3, 123.5, 123.1, 53.8, 48.7, 46.2, 42.2, 21.5, 13.7, 11.7 ppm. UV/Vis ((CH₃)₂CO): λ_{max}/nm (ε/M^{−1} cm^{−1}) 439 (280), 351 (6900), 345 (6900). HRMS found *m/z* 602.0682, calcd *m/z* 602.0682 for [C₂₀H₂₁N₃O₂AuCl + Cl]⁺. IR (solid) ν/cm^{−1}: 2959, 2882, 2357, 1691, 1651, 1585, 1520, 1470, 1423, 1383, 1362, 1344, 1333, 1267, 1234, 1190, 1065, 907, 833, 789, 644, 557, 482, 405, 382, 359, 334, 324, 318, 312, 301, 293, 284, 276, 257, 231, 220, 214.

Synthesis of [AuCl(L⁴)]. As for [AuCl(L¹)], but using [HL⁴]PF₆ (98 mg, 0.17 mmol), KO^tBu (19 mg, 0.17 mmol) and [AuCl(tht)] (53 mg, 0.17 mmol). The product was obtained as a grey solid (yield: 86 mg, 85%). ¹H NMR (500 MHz, CDCl₃): δ_H 8.56 (d, 1H, ³J_{HH} = 7.3 Hz), 8.50 (d, 1H, ³J_{HH} = 7.7 Hz), 8.25 (d, 1H, ³J_{HH} = 8.4 Hz), 7.83 (d, 1H, ³J_{HH} = 7.7 Hz), 7.73–7.69 (m, 1H), 7.65 (d, 2H, ³J_{HH} = 7.2 Hz), 7.31 (m, 3H), 4.40 (br. t, 2H), 4.15–3.80 (m, 4H), 1.78–1.69 (overlapping m, 2H), 0.98 (t, 3H, ³J_{HH} = 7.4 Hz) ppm. ¹³C NMR (126 MHz, CDCl₃): δ_C 192.3, 163.8, 163.3, 142.6, 140.0, 131.8, 131.3, 129.6, 129.2, 128.8, 128.0, 127.9, 127.8, 126.4, 123.5, 123.4, 123.2, 53.8, 52.5, 42.3, 21.5, 11.7 ppm. UV/Vis ((CH₃)₂CO): λ_{max}/nm (ε/M^{−1} cm^{−1}) 352 (11 760), 345 (11 860). HRMS found *m/z* 597.1551, calcd *m/z* 597.1559 for [C₂₄H₂₁N₃O₂AuCl-HCl + NH₄]⁺. IR (solid) ν/cm^{−1}: 2967, 2955, 2873, 1703, 1655, 1622, 1591, 1506, 1475, 1433, 1389, 1354, 1340, 1286, 1276, 1238, 1068, 1018, 958, 908, 858, 785, 764, 754, 692, 673, 588, 546.

Synthesis of [AuCl(L⁶)]. As for [AuCl(L¹)], but using [HL⁶]PF₆ (62 mg, 0.16 mmol), [AuCl(tht)] (57 mg, 0.16 mmol) and KO^tBu (17 mg, 0.16 mmol). The product was obtained as a grey solid (yield: 49 mg, 49%). ¹H NMR (400 MHz, CDCl₃): δ_H 8.67 (d, 1H, ³J_{HH} = 6.2 Hz), 8.62 (d, 1H, ³J_{HH} = 7.7 Hz), 8.32 (d, 2H, ³J_{HH} = 7.7 Hz), 7.91 (d, 1H, ³J_{HH} = 7.8 Hz), 7.86–7.76 (m, 1H), 7.73 (d, 2H, ³J_{HH} = 8.0 Hz), 7.54 (d, 2H, ³J_{HH} = 7.1 Hz), 7.47–7.30 (m, 5H), 5.42 (s, 2H), 4.48 (s, 2H), 4.10–3.65 (m, 4H) ppm. ¹³C{¹H} NMR (126 MHz, CDCl₃): δ_C 192.5, 164.8, 164.2, 163.8, 163.3, 149.4, 142.7, 139.9, 138.0, 137.2, 134.4, 132.2, 131.6, 131.5, 130.3, 129.6, 129.0, 128.9, 128.6, 128.5, 128.1, 127.7, 127.4, 126.4, 125.1, 125.0, 123.3, 122.7, 121.6, 120.9, 110.8, 104.0, 54.6, 54.5, 53.9, 53.8, 53.7, 52.3, 50.1, 45.4, 43.9, 43.5, 40.2, 25.7 ppm. UV/Vis ((CH₃)₂CO): λ_{max}/nm (ε/M^{−1} cm^{−1}) 436 (700), 343 (1600). HRMS found *m/z* 645.1549, calcd *m/z* 645.1559 for [C₂₈H₂₀AuN₃O₂ + NH₄]⁺. IR (solid) ν/cm^{−1}: 2961, 2914, 2845, 1703, 1682, 1655, 1580, 1522, 1508, 1472, 1454, 1425, 1402, 1383, 1312, 1260, 1236, 1177, 1136, 1069, 1016, 964, 845, 799, 785, 737, 704, 692, 617, 594, 583, 557, 544, 500, 480, 459, 436, 428, 417.

Synthesis of [AuCl(L⁷)]. As for [AuCl(L¹)], but using [HL⁷]PF₆ (86 mg, 0.16 mmol), KO^tBu (18 mg, 0.16 mmol) and [AuCl(tht)] (50 mg, 0.16 mmol). The product was obtained as a grey-yellow solid (yield: 68 mg, 68%). ¹H NMR (400 MHz, (CD₃)₂CO): δ_H 8.39 (app. d, 2H, ³J_{HH} = 7.5 Hz), 8.33 (d, 1H, ³J_{HH} = 7.6 Hz), 7.80 (d, 1H, ³J_{HH} = 8.7 Hz), 7.71 (app. t, 1H, ³J_{HH} = 7.5 Hz), 5.03–4.89 (m, 4H), 2.95–2.75 (m, 2H), 1.65–1.20 (m, 15H), 0.91 (t, 3H, ³J_{HH} = 6.0 Hz) ppm. ¹³C{¹H} NMR (126 MHz, (CD₃)₂CO): δ_C 193.8, 164.3, 163.8, 144.4, 132.1, 131.7, 130.4, 130.0, 129.7, 128.5, 127.1, 124.4, 123.7, 54.6, 49.5, 46.6, 40.9, 32.6, 30.2, 30.1, 28.7, 27.9, 23.3, 14.4, 13.9 ppm. UV/Vis ((CH₃)₂CO): λ_{max}/nm (ε/M^{−1} cm^{−1}) 439 (340), 351 (4360), 345 (4360). HRMS found *m/z* 660.1678, calcd *m/z* 660.1663 for [C₂₅H₃₁AuClN₃O₂ + Na]⁺. IR (solid) ν/cm^{−1}: 3341, 2920, 2854, 2110, 1703, 1657, 1585, 1531, 1470, 1429, 1391, 1350, 1275, 1234, 1096, 856, 729, 478.

Synthesis of [AuCl(L⁸)]. As for [AuCl(L¹)], but using [HL⁸]PF₆ (70 mg, 0.16 mmol), [AuCl(tht)] (50 mg, 0.16 mmol) and KO^tBu (18 mg, 0.16 mmol). The product was obtained as a grey



coloured solid (yield: 31 mg, 79%). ^1H NMR (500 MHz, CD_3CN): δ_{H} 8.63 (d, 2H, $^3J_{\text{HH}} = 7.4$ Hz), 8.57 (d, 1H, $^3J_{\text{HH}} = 8.6$ Hz), 8.00 (d, 1H, $^3J_{\text{HH}} = 7.2$ Hz), 7.93 (app. t, 1H, $^3J_{\text{HH}} = 7.8$ Hz), 7.82 (d, 2H, $^3J_{\text{HH}} = 7.8$ Hz), 7.52 (app. t, 2H, $^3J_{\text{HH}} = 7.4$ Hz), 7.42 (app. t, 1H, $^3J_{\text{HH}} = 7.1$ Hz), 5.18 (br s, 2H), 4.45 (br. t, 2H), 4.32 (br. t, 2H), 4.10 (t, 2H, $^3J_{\text{HH}} = 7.5$ Hz), 2.85–2.75 (m, 2H), 1.44–1.22 (m, 10H), 0.88 (t, 3H, $^3J_{\text{HH}} = 6.0$ Hz) ppm. ^{13}C $\{^1\text{H}\}$ NMR (126 MHz, CDCl_3): δ_{C} 192.8, 163.8, 163.3, 142.4, 140.0, 132.0, 131.3, 129.7, 129.4, 128.6, 128.1, 128.1, 128.0, 126.4, 123.7, 123.5, 123.3, 66.0, 53.7, 52.3, 40.9, 32.0, 29.5, 29.4, 28.3, 27.3, 22.8, 15.4, 14.2 ppm. UV/Vis ($(\text{CH}_3)_2\text{CO}$): λ_{max} /nm ($\epsilon/\text{M}^{-1}\text{cm}^{-1}$) 441 (3380), 351 (14 160), 344 (14 560). HRMS found m/z 650.2071, calcd m/z 650.2076 for $[\text{C}_{29}\text{H}_{31}\text{AuN}_3\text{O}_2-\text{Cl}]^+$. IR (solid) ν/cm^{-1} : 3059, 2949, 2918, 2851, 1703, 1655, 1620, 1589, 1502, 1477, 1438, 1404, 1392, 1357, 1340, 1321, 1288, 1234, 1176, 1097, 1074, 1045, 1024, 858, 785, 754, 692, 671, 651, 613, 584, 559, 543, 482, 410.

Conflicts of interest

There are no conflicts to declare.

Acknowledgements

We thank Cardiff University for an Endowment Studentship and EPSRC for DTP funding (L. M. G.). Dr C. Williams holds a Sêr Cymru II Fellowship part funded by the European Regional Development Fund through the Welsh Government. The EPSRC Mass Spectrometry National Service (Swansea University) and EPSRC National Crystallographic Service (University of Southampton) are also thanked. Dr E. Lloyd-Evans and Dr P. Watson (Cardiff University) are thanked for commercial fluorophores and Mr H. Mottram for cytotoxicity data.

Notes and references

- G. J. Higby, *Gold Bull.*, 1982, **15**, 130; P. J. Sadler, *Struct. Bonding*, 1976, **29**, 171.
- S. Nobili, E. Mini, I. Landini, C. Gabbiani, A. Casini and L. Messori, *Med. Res. Rev.*, 2010, **30**, 550.
- K. D. Mjos and C. Orvig, *Chem. Rev.*, 2014, **114**, 4540.
- S. J. Berners-Price and A. Filipovska, *Metallomics*, 2011, **3**, 863.
- E. R. T. Tiekink, *Crit. Rev. Oncol. Hematol.*, 2002, **42**, 225; S. S. Gunatilleke and A. M. Barrios, *J. Med. Chem.*, 2006, **49**, 3933.
- S. B. Aher, P. N. Muskawar, K. Thenmozhi and P. R. Bhagat, *Eur. J. Med. Chem.*, 2014, **81**, 408; A. Gautier and F. Cisnetti, *Metallomics*, 2012, **4**, 23; H. G. Raubenheimer and S. Cronje, *Chem. Soc. Rev.*, 2008, **37**, 1998; J. F. Arambula, R. McCall, K. J. Sidoran, D. Magda, N. A. Mitchell, C. W. Bielawski, V. M. Lynch, J. L. Sessler and K. Arumugam, *Chem. Sci.*, 2016, **7**, 1245.
- (a) L. E. Wedlock and S. J. Berners-Price, *Aust. J. Chem.*, 2011, **64**, 692; (b) L. E. Wedlock, M. R. Kilburn, J. B. Cliff, L. Filgueira, M. Saunders and S. J. Berners-Price, *Metallomics*, 2011, **3**, 917; (c) O. Karaca, V. Scalcon, S. M. Meier-Menches, R. Bonsignore, J. M. J. L. Brouwer, F. Tonolo, A. Folda, M. P. Rigobello, F. E. Kuhn and A. Casini, *Inorg. Chem.*, 2017, **56**, 14237.
- E. E. Langdon-Jones and S. J. A. Pope, *Chem. Commun.*, 2014, **50**, 10343.
- J. J. Dunsford, K. J. Cavell and B. M. Kariuki, *Organometallics*, 2012, **31**, 4118; P.-H. Lanoe, B. Najjari, F. Hallez, G. Gontard and H. Amouri, *Inorganics*, 2017, **5**, 58.
- (a) R. J. Ditchfield, *J. Chem. Phys.*, 1972, **56**, 5688; (b) A. M. Lee, N. C. Handy and S. M. Colwell, *J. Chem. Phys.*, 1995, **103**, 10095.
- A. M. Sarotti and S. C. Pellegrinet, *J. Org. Chem.*, 2009, **74**, 7254.
- H. Schmidbaur and A. Schier, *Chem. Soc. Rev.*, 2012, **41**, 370.
- (a) S. Banerjee, E. B. Veale, C. M. Phelan, S. A. Murphy, G. M. Tocci, L. J. Gillespie, D. O. Frimannsson, J. M. Kelly and T. Gunnlaugsson, *Chem. Soc. Rev.*, 2013, **42**, 1601.
- A. Vlček and S. Zalis, *Coord. Chem. Rev.*, 2007, **251**, 258.
- D. Jacquemin, E. A. Perpète, G. Scalmani, I. Ciofini, C. Peltier and C. Adamo, *Chem. Phys.*, 2010, **372**, 61.
- P. J. Stephens and H. Nobuyuki, *Chirality*, 2010, **22**, 229.
- P. J. Barnard, M. V. Baker, B. W. Skelton, A. H. White and S. J. Berners-Price, *J. Inorg. Biochem.*, 2003, **96**, 99; P. J. Barnard, M. V. Baker, S. J. Berners-Price and D. A. Day, *J. Inorg. Biochem.*, 2004, **98**, 1642.
- I. Özdemir, A. Denizci, H. T. Öztürk and B. Çetinkaya, *Appl. Organomet. Chem.*, 2004, **18**, 318.
- (a) J. L. Hickey, R. A. Ruhayel, P. J. Barnard, M. V. Baker, S. J. Berners-Price and A. Filipovska, *J. Am. Chem. Soc.*, 2008, **130**, 12570; (b) B. A. Stanley, V. Sivakumaran, S. Shi, I. McDonald, D. Lloyd, W. H. Watson, M. A. Aon and N. Paolocci, *J. Biol. Chem.*, 2011, **286**, 33669; (c) C. F. Williams, N. Yarlett, M. A. Aon and D. Lloyd, *Mol. Biochem. Parasitol.*, 2014, **196**, 45.
- R. Visbal, V. Fernández-Moreira, I. Marzo, A. Laguna and M. C. Gimeno, *Dalton Trans.*, 2016, **45**, 15026.
- A. Meyer, L. Oehninger, Y. Geldmacher, H. Alborzinia, S. Wölfl, W. S. Sheldrick and I. Ott, *ChemMedChem*, 2014, **9**, 1794.
- M. Porchia, M. Pellei, M. Marinelli, F. Tisato, F. Del Bello and C. Santini, *Eur. J. Med. Chem.*, 2018, **146**, 709.
- L. A. Mullice, H. J. Mottram, A. J. Hallett and S. J. A. Pope, *Eur. J. Inorg. Chem.*, 2012, 3054.
- C. Carporale, C. A. Bader, A. Sorvina, K. D. M. Magee, B. W. Skelton, T. A. Gillam, P. J. Wright, P. Raiteri, S. Stagni, J. L. Morrison, S. E. Plush, D. A. Brooks and M. Massi, *Chem. – Eur. J.*, 2017, **23**, 15666.
- V. Fiorini, I. Zannoni, A. L. Costa, A. Hochkoeppler, V. Zanolli, A. Ranieri, M. Masi, A. Stefan and S. Stagni, *Dalton Trans.*, 2017, **46**, 12328.



- 26 For recent examples: L. H. Davies, R. W. Harrington, W. Clegg and L. J. Higham, *Dalton Trans.*, 2014, **43**, 13485; A. Meyer, C. P. Bagowski, M. Kokoschka, M. Stefanopoulou, H. Alborzinia, S. Can, D. H. Vlecken, W. S. Sheldrick, S. Wölfl and I. Ott, *Angew. Chem., Int. Ed.*, 2012, **51**, 8895.
- 27 M. E. Garner, W. Niu, X. Chen, I. Ghiviriga, K. A. Abboud, W. Tan and A. S. Veige, *Dalton Trans.*, 2015, **44**, 1914.
- 28 G. D. Frey, R. D. Dewhurst, S. Kousar, B. Donnadiou and G. Bertrand, *J. Organomet. Chem.*, 2008, **693**, 1674.
- 29 M. Frank, M. Nieger, F. Vogtle, P. Belser, A. von Zelewsky, L. De Cola, V. Balzani, F. Barrigelletti and L. Flamigni, *Inorg. Chim. Acta*, 1996, **242**, 281.
- 30 S. J. Coles and P. A. Gale, *Chem. Sci.*, 2012, **3**, 683.
- 31 *CrystalClear-SM Expert 3.1 b27*, Rigaku, 2013.
- 32 *CrystAlisPro 1.171.38.41*, Rigaku Oxford Diffraction, 2015.
- 33 O. V. Dolomanov, L. J. Bourhis, R. J. Gildea, J. A. K. Howard and H. Puschmann, *J. Appl. Crystallogr.*, 2009, **42**, 339.
- 34 G. M. Sheldrick, *Acta Crystallogr., Sect. A: Found. Adv.*, 2015, **71**, 3.
- 35 G. M. Sheldrick, *Acta Crystallogr., Sect. C: Struct. Chem.*, 2015, **27**, 3.
- 36 L. Palatinus and G. Chapuis, *J. Appl. Crystallogr.*, 2007, **40**, 786.
- 37 T. Mosmann, *J. Immunol. Methods*, 1983, **65**, 55.
- 38 M. J. Frisch, G. W. Trucks, H. B. Schlegel, G. E. Scuseria, M. A. Robb, J. R. Cheeseman, G. Scalmani, V. Barone, B. Mennucci, G. A. Petersson, H. Nakatsuji, M. Caricato, X. Li, H. P. Hratchian, A. F. Izmaylov, J. Bloino, G. Zheng, J. L. Sonnenberg, M. Hada, M. Ehara, K. Toyota, R. Fukuda, J. Hasegawa, M. Ishida, T. Nakajima, Y. Honda, O. Kitao, H. Nakai, T. Vreven, J. A. Montgomery Jr., J. E. Peralta, F. Ogliaro, M. Bearpark, J. J. Heyd, E. Brothers, K. N. Kudin, V. N. Staroverov, T. Keith, R. Kobayashi, J. Normand, K. Raghavachari, A. Rendell, J. C. Burant, S. S. Iyengar, J. Tomasi, M. Cossi, N. Rega, J. M. Millam, M. Klene, J. E. Knox, J. B. Cross, V. Bakken, C. Adamo, J. Jaramillo, R. Gomperts, R. E. Stratmann, O. Yazyev, A. J. Austin, R. Cammi, C. Pomelli, J. W. Ochterski, R. L. Martin, K. Morokuma, V. G. Zakrzewski, G. A. Voth, P. Salvador, J. J. Dannenberg, S. Dapprich, A. D. Daniels, O. Farkas, J. B. Foresman, J. V. Ortiz, J. Cioslowski and D. J. Fox, *Gaussian 09, Revision C.01*, Gaussian Inc., Wallingford CT, 2010.
- 39 C. Adamo and V. Barone, *J. Chem. Phys.*, 1999, **110**, 6158.
- 40 R. Krishnan, J. S. Binkley, R. Seeger and J. A. Pople, *J. Chem. Phys.*, 1980, **72**, 650.
- 41 D. Andrae, U. Häußermann, H. Stoll and H. Preuß, *Theor. Chim. Acta*, 1990, **77**, 123.
- 42 J. Tomasi, B. Mennucci and R. Cammi, *Chem. Rev.*, 2005, **105**, 2999.
- 43 (a) E. E. Langdon-Jones, D. Lloyd, A. J. Hayes, S. D. Wainwright, H. J. Mottram, S. J. Coles, P. N. Horton and S. J. A. Pope, *Inorg. Chem.*, 2015, **54**, 6606; (b) E. E. Langdon-Jones, N. O. Symonds, S. E. Yates, A. J. Hayes, D. Lloyd, R. Williams, S. J. Coles, P. N. Horton and S. J. A. Pope, *Inorg. Chem.*, 2014, **53**, 3788.
- 44 R. Uson, A. Laguna and J. Vicente, *J. Organomet. Chem.*, 1977, **131**, 471.

